Hindawi
Advances in Civil Engineering
Volume 2019, Article ID 8214534, 20 pages
https://doi.org/10.1155/2019/8214534

Research Article

Effect of Basalt Fiber Addition on Static-Dynamic Mechanical Behaviors and Microstructure of Stabilized Soil Compositing Cement and Fly Ash

Ziming Cao,[1,2] **Qinyong Ma**,[1,2,3] **and Hongwei Wang**[1,2]

[1]*School of Civil Engineering and Architecture, Anhui University of Science and Technology, Huainan, Anhui 232001, China*
[2]*Engineering Research Center of Underground Mine Construction, Ministry of Education, Anhui University of Science and Technology, Huainan, Anhui 232001, China*
[3]*State Key Laboratory of Mining Response and Disaster Prevention and Control in Deep Coal Mine, Anhui University of Science and Technology, Huainan, Anhui 232001, China*

Correspondence should be addressed to Ziming Cao; ziming_cao@foxmail.com

Received 15 July 2019; Revised 14 October 2019; Accepted 19 October 2019; Published 11 November 2019

Academic Editor: Marco Corradi

The purpose of this article is to evaluate the influence of basalt fiber content on the static-dynamic mechanical properties and microstructure of cement-fly ash-stabilized soil. The optimum mixed contents of cement and fly ash were obtained from the results of a series of physical and mechanical experiments. Based on the optimum mixed contents of cement and fly ash, the static-dynamic mechanical performances and microstructure of cement-fly ash-stabilized soil reinforced with basalt fiber were studied by means of the unconfined compression test, dynamic compression test (namely, SHPB test), and SEM test. The results demonstrated that the addition of basalt fiber in cement-fly ash-stabilized soil significantly enhanced the static-dynamic mechanical properties of stabilized soil. With basalt fiber content varying from 0% to 1.2%, the unconfined compressive strength, dynamic compressive strength, dynamic increase factor, and specific energy absorption of stabilized soil showed an upward trend first and a downward trend subsequently. The unconfined compressive strength, dynamic compressive strength, and energy absorption ability have a maximum improvement under the optimum basalt fiber content of 0.6%. In addition, the inclusion of basalt fiber can change the failure pattern of cement-fly ash-stabilized soil. The fractal dimension of broken fragments decreased gradually with the increasing basalt fiber content and increased correspondingly with the increasing impact loading pressure. With the basalt fiber content of 0.6%, a stable internal space structure produced inside stabilized soil. However, there are many fiber-fiber weak interfaces that appeared inside stabilized soil under the basalt fiber content of 1.2%. The microstructural observations can be considered as the good interpretations to verify the macroscopic mechanical characteristics.

1. Introduction

Soil stabilization technique is a common method for the modification and improvement of the various properties of expansive soil [1]. Expansive soil generally poses a volume change behavior due to the variation of moisture content in the soil [2, 3]. Therefore, this particular property can easily bring out serious problems to several engineering constructions, such as foundation, road, embankment, and railway [1–3]. Previous investigations by many researchers have observed that the soil stabilization technique produced a significant improvement in terms of geotechnical properties, which include swelling-shrinkage, compaction, plasticity, compressibility, and strength properties [4–7]. The soil stabilization methods usually include the chemical stabilization, physical stabilization, and a combination of these two treatments. It is well known that the combination method of physical and chemical stabilization is widely applied in geotechnical engineering to create mixed soil materials that possess a good characteristic [8]. Chemical stabilizations were used to obtain an enhancement in soil strength and a reduction in the swelling behavior of expansive soil [7, 9].

Besides, many researchers have found that the physical stabilizations also can improve the strength of expansive soil and mitigate its expansion. The cation exchange reaction, flocculation, and pozzolanic reaction occurred inside the soil matrix with the addition of chemical stabilizers such as lime, cement, and fly ash [6, 10–13]. With a further improvement in the engineering properties of stabilized soil with various chemical additives, the utilization of physical additive (such as fiber or sand) is a good measure to improve the chemical additive-treated soil.

In the past, many studies with respect to the stabilization and modification of expansive soil found the mechanisms and the change rule of soil treated with various stabilizers. Çokça [14] and Phanikumar and Sharma [15] observed that the utilization of fly ash in expansive soil stabilization can obtain the desired results in reducing the swelling behaviors and improving the compaction and strength characteristics. Moreover, the pozzolanic reaction, cation exchange effect, and the formation of cementitious compounds are the reasons of the reduction in swelling properties and the variation in physical-mechanical behaviors of fly ash-treated soil. Various additives have different effectiveness on the strength behaviors and expansibility of stabilized soil. Punthutaecha et al. [16] performed many research tests about the effects of ashes and fibers on volume change behavioral properties of expansive soil and found that the combination of ashes and fibers under their optimum contents can reach a considerable improvement in soil properties when compared with soil treated with only one stabilizer. The study results of Sharma et al. [17] indicated that the three stabilizers of lime, calcium chloride, and rice husk ash all present an obvious influence on unconfined compressive strength. The corresponding optimum content of different stabilizers can be acquired by the unconfined compression test and California bearing ratio test. In addition, Jha and Sivapullaiah [7] carried out the scanning electron microscopy tests and observed that the improvement in soil strength is a macroscopic result of the formation of cementitious compounds inside soil micropores and the binding of soil particles by cementitious gel. Phanikumar and Singla [18] investigated the effects of fiber content and fiber length on the swelling behaviors of expansive soil. The test results showed that the swelling potential and the vertical swelling pressure of stabilized soil both have a decreasing trend with the increase in fiber content or fiber length. The investigations performed by Yazdandoust and Yasrobi [19] showed that the wetting-drying cycles have an influence on the untreated soil and polymer-treated soil, but the addition of polymer into soil samples can effectively alleviate and control the detrimental effect of cyclic wetting-drying. Moreover, Kalkan [20] adopted the stabilizer of silica fume to reduce the effect of cyclic wetting-drying condition on plasticity and swelling properties of expansive soil, and the experimental results showed that the stabilization technique of usage of silica fume has a beneficial effect in terms of soil improvement. For improving the properties of expansive soil, Dayioglu et al. [21] selected the class C fly ash, class F fly ash, and lime as the stabilizers to treat the original expansive soil, and the swelling pressure tests and unconfined compression tests were conducted on mixed soil samples. Besides, the influences of freeze-thaw cycles on strength behaviors and expansion of stabilized soil with different additives were studied and analyzed. Por et al. [22] researched the effect of cement stabilizer on deformation behaviors and stress responses of expansive soil under swelling and found that the cement-treated soil presents an obvious improvement in soil strength and stiffness. In addition, the cement stabilization method can effectively reduce the swelling-shrinkage properties of expansive soil. As reported by Zhao et al. [23], the free swelling ratio of highly expansive soil treated with cement shows a decreasing trend. The improvement in strength is attributed to the newly generated cementitious materials, which can result in the cementation among dispersive soil particles and filling of micropores. This observation is similar to the experimental results of Por et al. [22]. The relevant research [24] indicated that the construction technique of cement-treated expansive soil is widely applied in practical engineering, such as expansive soil area in the Middle Route of South-to-North Water Diversion Project of China. Because the effectiveness of cement stabilization on expansive soil is better than lime stabilization and the environmental pollution of cement treatment is relatively small [24, 25], the stabilizer of cement is chosen in the following research. In consideration of cost-effectiveness, environmental protection, and waste utilization [6, 15], the industrial waste material of fly ash should be adopted simultaneously in this study. For soil stabilization of cement and fly ash mixtures, the cement can be regarded as a chemical activator for fly ash to obtain more conspicuous improvement of stabilized soil [26]. Thus, the chemical stabilizers of cement and fly ash are selected together in the present investigation. According to previous studies [8, 16, 27], the physical additive of fiber can further improve the various behaviors of stabilized soil with chemical additive. Therefore, the effect of fiber reinforcement on the properties of stabilized soil is worth considering.

The achievements obtained from the above literatures mostly concentrated on the swelling behaviors, plasticity, compaction, and static strength of stabilized soil. In addition, the above studies have analyzed the effect of cyclic wetting-drying and cyclic freeze-thaw phenomena on stabilized soil. In practical engineering, the stabilized soils are not only subjected to static loading [2, 4, 7, 15, 17], wetting-drying cycles [10, 19, 20], and freeze-thaw cycles [21] but also subjected to impact loading [27]. For instance, in the construction of national defense engineering, the geomaterials of stabilized soil were usually subjected to strong dynamic loading, such as impacting and explosion [28]. Moreover, the stabilized expansive soil was used as a filling material for the subgrade layer of airport runway in the construction of airfield infrastructure [29]. When the airplane comes down to the airport runway, it directly induces a severe impacting on the road surface and the foundation soil layer of airport runway. Currently, there are relatively few studies with respect to the dynamic behaviors of stabilized soil under impact loading. Therefore, the research of the dynamic properties of stabilized soil under impact loading appears very imperative and significant. What is more, the

dynamic mechanical behaviors of stabilized soil can be comprehensively analyzed as they combined with the static mechanical behaviors.

The current research work aims to investigate the static-dynamic mechanical properties and microstructure of cement-fly ash-stabilized soil reinforced with basalt fiber. At first, the original expansive soil was treated with cement and fly ash to study the influence of cement-fly ash admixtures on swelling-shrinkage behaviors, Atterberg limits, and unconfined compressive strength. The purpose of the above experimental studies is to obtain the optimum mixed contents of cement and fly ash. Next, based on the optimum mixed contents of cement and fly ash, an attempt has been made to evaluate the addition of basalt fiber on the static-dynamic mechanical behaviors of cement-fly ash-stabilized soil, which was performed by unconfined compression test and split Hopkinson pressure bar (SHPB) test. To verify the effect of basalt fiber addition on the behaviors of cement-fly ash-stabilized soil more accurately, the scanning electron microscopy (SEM) test on stabilized soil samples was carried out. Through the SEM observation results and the experimental data obtained from unconfined compression test and SHPB test, the fiber reinforcement effect on various characteristics of cement-fly ash-stabilized soil was analyzed and discussed comprehensively. These characteristics include static stress-strain curve, unconfined compressive strength, dynamic stress-strain curve, dynamic compressive strength, dynamic increase factor (DIF), energy absorption, failure pattern, fractal property, and microstructure. Finally, it can be clearly observed that the influence of basalt fiber addition on static-dynamic mechanical properties and microstructure of cement-fly ash-stabilized soil.

2. Materials and Methods

2.1. Materials

2.1.1. Soil Characteristics. The original soil material used in this investigation was obtained from a construction site of metro line in Hefei, Anhui Province, China. The grain size distribution of selected soil is presented in Figure 1. The liquid limit, plastic limit, and plasticity index of original soil were 42.8%, 22.0%, and 20.8, respectively. Besides, the engineering property indices of selected soil were tested according to GB/T 50123-1999 Standard for Soil Test Method [30] and are shown in Table 1.

2.1.2. Cement. The chemical stabilizer of cement applied in this study was obtained from a cement plant situated in Huainan, Anhui Province, China. In addition, the selected cement is Portland cement (PO 42.5) with measured compressive strengths of 25.8 MPa (3 days) and 53.5 MPa (28 days) and flexural strengths of 5.3 MPa (3 days) and 8.2 MPa (28 days), respectively. The specific surface of cement is 372 m^2/kg. The initial setting time and final setting time of cement are 155 minutes and 205 minutes, respectively.

2.1.3. Fly Ash. The soil-stabilizing agent of fly ash was collected from a power plant located in Huainan, Anhui Province, China. The main constituents of the selected fly ash are SiO_2, Al_2O_3, Fe_2O_3, and CaO. The percentages of SiO_2, Al_2O_3, Fe_2O_3, and CaO are 40.12, 23.58, 7.39, and 9.65, respectively. The other constituents have the percentage of 19.26. Based on the chemical compositions of fly ash used in the present study, it can be classified as class F fly ash in accordance with the ASTM C618 Standard Specification [31].

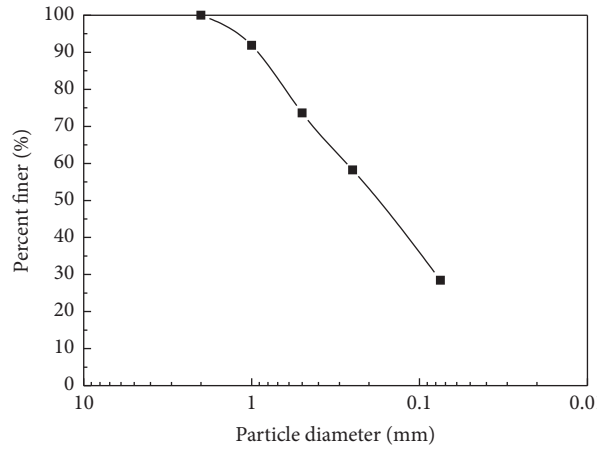

Figure 1: Grain size distribution curve of original expansive soil.

2.1.4. Basalt Fiber. As a green environmental protection material, basalt fiber is manufactured from natural basalt due to wire drawing technique, and it is mainly composed of SiO_2, Al_2O_3, CaO, MgO, Fe_2O_3, and TiO_2 [32]. Furthermore, basalt fiber has been widely used in many research fields because of its high strength, excellent corrosion resistance, flame resistance, and chemical resistance [27, 32]. Therefore, the fiber reinforcement method for the stabilized soil in this study selected basalt fiber. The basalt fiber used in the present research is exhibited in Figure 2. The physical and mechanical performances of basalt fiber are given in Table 2.

2.2. Specimen Preparation. In this investigation, the preparation processes of stabilized soil specimens can comply with the method mentioned in Ref. [2]. Initially, the dried soil (with a constant temperature of 105°C for more than 24 h) was crushed down by the hammer and passed through a 2 mm sieve. Second, the predetermined amount of oven-dried soil sample powder was thoroughly mixed with different additives in the dry state. Subsequently, the required amount of distilled water was uniformly sprayed on the soil-additive mixtures and mixed again by the automatic mixer. To ensure the complete mixing of soil and additives, the time of mixing process was fixed at 5 minutes. All the mixing procedures were finished, and then the appropriate curing measure was taken to achieve moisture equilibrium. According to the method mentioned in the relevant researches [2, 6, 9, 11], the soil-additive mixtures were kept in a closed container and stored at a temperature of 20°C ± 2°C for 24 h to satisfy the condition of moisture equilibrium. After that, the mixtures were placed into a standard mould. For static compression test (namely, unconfined compression

Table 1: Engineering property indices of original soil used in the study.

Liquid limit (%)	Plastic limit (%)	Plasticity index (%)	Specific gravity	Optimum moisture content (%)	Maximum dry density (g/cm^3)	Free swelling ratio (%)
42.8	22.0	20.8	2.71	18.9	1.76	46

Table 2: Physical and mechanical properties of basalt fiber.

Average length (mm)	Filament diameter (μm)	Density (g/cm^3)	Elasticity modulus (GPa)	Tensile strength (GPa)	Elongation at break (%)
9	13	2.7	90–110	4.0–4.8	3.2

Figure 2: Photograph of basalt fiber.

test), the mixtures were compacted at least 5 layers in the compaction mould with 50 mm in diameter and 100 mm in height. For dynamic uniaxial compression test (namely, SHPB test), the mixtures were compacted at least 3 layers in the compaction mould with 50 mm in diameter and 25 mm in height. Under each experimental condition, the soil-additive mixtures were prepared with the optimum moisture content of 18.9% and the maximum dry density of 1.76 g/cm^3. At last, the freshly prepared specimens were taken out from the compaction mould and cured in a standard curing chamber with a relative humidity of 95% ± 3% and a temperature of 20°C ± 2°C for the given curing age.

For a series of physical and mechanical tests, the one group is about the soil samples stabilized with varying contents of cement of 0%, 2%, 4%, 6%, and 8%. Based on the previous studies [25, 33], with the addition of excess cement into the soil sample, the improvement of stabilized soil in swelling-shrinkage behaviors was not obvious. In addition, the inclusion of excess cement into soil will cause a phenomenon of environmental pollution. Thus, the cement content was selected at 5% for the following research. After that, another group includes the soil samples treated with the given cement content (C) of 5% and different fly ash contents (FA) of 0%, 5%, 10%, 15%, and 20%. After preliminary research of swelling-shrinkage, plasticity, and strength behaviors of cement-fly ash-stabilized soil, the effect of basalt fiber on the static-dynamic behaviors of cement-fly ash-stabilized soil was investigated. The five types of cement-fly ash-stabilized soil specimens were prepared for the unconfined compression test and SHPB test, with basalt fiber contents (BF) of 0%, 0.3%, 0.6%, 0.9%, and 1.2% by weight of dry soil. For the unconfined compression test, three specimens were fabricated for each basalt fiber dosage. For the SHPB test, five specimens were prepared for each basalt fiber dosage.

2.3. Testing Apparatus and Methods. Experiments to determine the free swelling ratio and volume shrinkage ratio were conducted on cement stabilized soil samples and cement-fly ash-stabilized soil samples according to GB/T 50123-1999 Standard for Soil Test Method [30]. The Atterberg limits test was carried out to make an assessment on the plasticity feature of untreated soil and chemical stabilizer-treated soil. The Atterberg limits test of cement stabilized soil samples and cement-fly ash-stabilized soil samples was performed using the combined liquid-plastic limit tester, in accordance with GB/T 50123-1999 Standard for Soil Test Method [30].

The unconfined compressive strength of soil specimen was determined by the experimental procedures described in GB/T 50123-1999 Standard for Soil Test Method [30]. The unconfined compression tests were carried out with a routine strain-controlled uniaxial compression testing machine at a constant loading rate of 1.0 mm/min. The cylindrical soil samples used in unconfined compression tests have a dimension of 50 mm diameter and 100 mm height. The static strength characteristics of soil specimens were measured with the unconfined compression test.

The SHPB tests (dynamic uniaxial compression tests) of fiber-reinforced cement-fly ash-stabilized soil were carried out through the 50 mm diameter SHPB apparatus. The SHPB apparatus presented in Figure 3 includes launch device, laser speedometer, striker bar, incident bar, transmitted bar, buffer device, strain gauge, semiconductor strain gauge, dynamic data acquisition system, and data processing system. Pressure bars manufactured with high-strength alloy steel (incident bar and transmitted bar) have a diameter of 50 mm. The density and elastic modulus of pressure bars are 7900 kg/m^3 and 210 GPa. The stabilized soil specimen was treated with lubricant and installed between the incident bar and transmitted bar prior to the SHPB test. Because stabilized soil belongs to the low wave impedance material, the application of strain gauge cannot capture an effective signal of transmitted wave. Currently, the semiconductor strain gauge technology has been widely applied in SHPB tests to obtain an effective signal of transmitted wave of low wave impedance materials [33–36]. Therefore, the usage of semiconductor strain gauge in SHPB tests makes it easier to

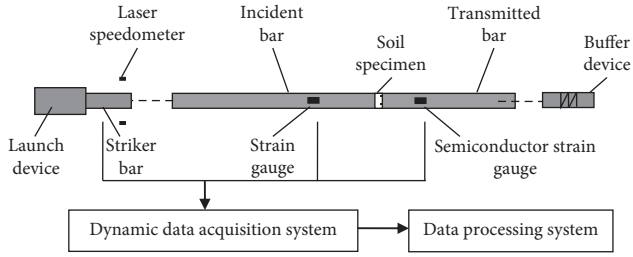

Figure 3: SHPB apparatus.

collect the effective signal of transmitted wave. For the SHPB apparatus presented in Figure 3, the strain gauge was mounted on the incident bar to collect the incident wave signal and reflected wave signal, and the semiconductor strain gauge was mounted on the transmitted bar to acquire the transmitted wave signal. According to the previous studies [27, 37], the three impact loading pressures of 0.3 MPa, 0.4 MPa, and 0.5 MPa were selected in SHPB tests. The corresponding strain rates of the impact loading pressure 0.3, 0.4, and 0.5 MPa are approximately 130 s^{-1}, 185 s^{-1}, and 220 s^{-1}.

To realize the uniform stress hypothesis in SHPB experiments of stabilized soil, some measures were adopted in this study: (1) the optimal slenderness ratio of soil specimen was 0.5 as suggested; (2) sufficient lubricant was smeared on the surface of the soil specimens to alleviate the end surface friction between specimen and bars; (3) the pulse shaping technique or spindle-shaped striker bar was used to obtain a smooth waveform. Based on above methods, the original waveforms (0.4 MPa impact loading pressure) obtained from SHPB tests are presented in Figure 4. It is clearly observed that the waveforms are smooth.

SEM experiments were carried out by a Quanta FEG 650 scanning electron microscope. All the SEM soil samples were kept in a dryer for the drying treatment. After that, the SEM soil samples were gold coated by a sputtering technique and installed in the scanning electron microscope before the SEM observations.

3. Results and Discussion

3.1. Effect of Chemical Additives on Index Properties of Stabilized Soil. Figure 5 shows the variations of swelling-shrinkage behaviors with cement content under different curing periods. All the cement-stabilized soil specimens were tested for 7 days and 28 days curing ages. It can be found in Figure 5 that the free swelling ratio and volume shrinkage ratio of stabilized soil decrease remarkably with the increase in cement content in experimental conditions of two curing periods. However, the variation trends of free swelling ratio and volume shrinkage ratio are not obvious with the cement content increased from 6% to 8%. Therefore, the excess additive of cement does not reduce the swelling-shrinkage properties of stabilized soil. The variations of swelling-shrinkage properties tend to be flat. To reduce the cost of stabilization and solve the serious environmental pollution, the industrial waste material of fly ash is mixed with cement for the next study. According to the

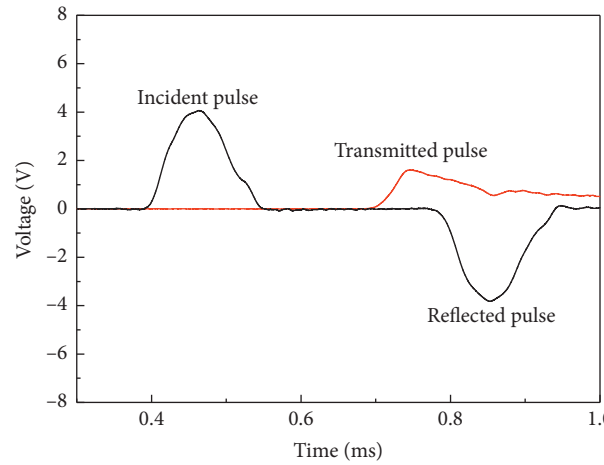

Figure 4: Original waveforms of SHPB test.

previous investigations [25, 33] and the preceding analysis, the cement content is chosen at 5% in the subsequent researches.

Figure 6 illustrates the variations of swelling-shrinkage behaviors with cement content (C) and fly ash content (FA) under different curing periods. With the given cement content of 5%, the free swelling ratio and volume shrinkage ratio of stabilized soil decrease with an increase in fly ash content when cement-fly ash-stabilized soil samples are cured for 7 and 28 days. With further increase in fly ash content, the free swelling ratio and volume shrinkage ratio of stabilized soil changed gently. The reduction of swelling-shrinkage properties due to the influences of the generation of hydration products inside stabilized soil and the cation exchange reactions between soil particles and fly ash [9, 21, 23, 35]. The principle of cement stabilization is similar to the above explanations. With the addition of more cement or fly ash into stabilized soil, the unreacted cement or fly ash particles kept inside stabilized soil are the main reason of the gentle variation phase in Figures 5 and 6 [38]. In addition, it is easily found that the curing period is another important factor to affect the mitigation of swelling-shrinkage properties of stabilized soil. This is similar to the findings of previous researches [4, 9, 21].

Liquid limit, plastic limit, and plasticity index of cement stabilized soil are exhibited in Figure 7. According to Figure 7, it can be observed that the cement treatment has a positive effect on reducing the liquid limit and plasticity index. The addition of 8% cement resulted in a maximum reduction in the plasticity index of stabilized soil. However, the plasticity index changes gently when the cement content increased from 6% to 8%. Thus, the excess additive of cement has a slight influence on the reduction of plasticity index. In the following investigation, the additive of fly ash was selected to replace a certain percentage of cement.

The Atterberg limits of cement-fly ash-stabilized soil under different curing periods are presented in Figure 8. With the cement content of 5%, the liquid limit and plasticity index have a decreasing trend with an increase in fly ash content. Besides, the liquid limit and plasticity index has

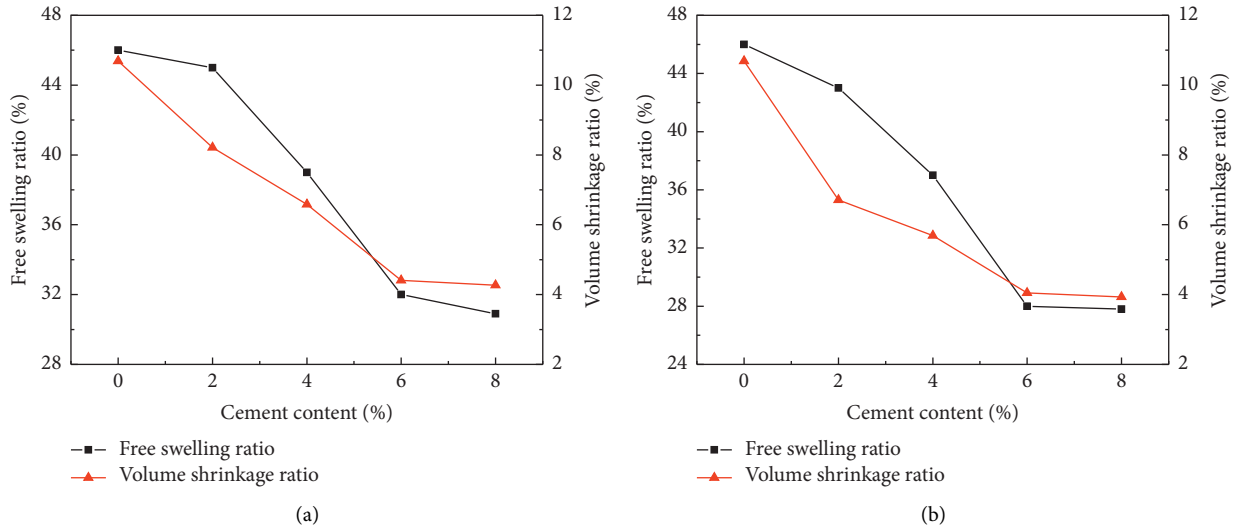

Figure 5: Swelling-shrinkage behaviors of cement-stabilized soil under different curing periods. (a) 7 days. (b) 28 days.

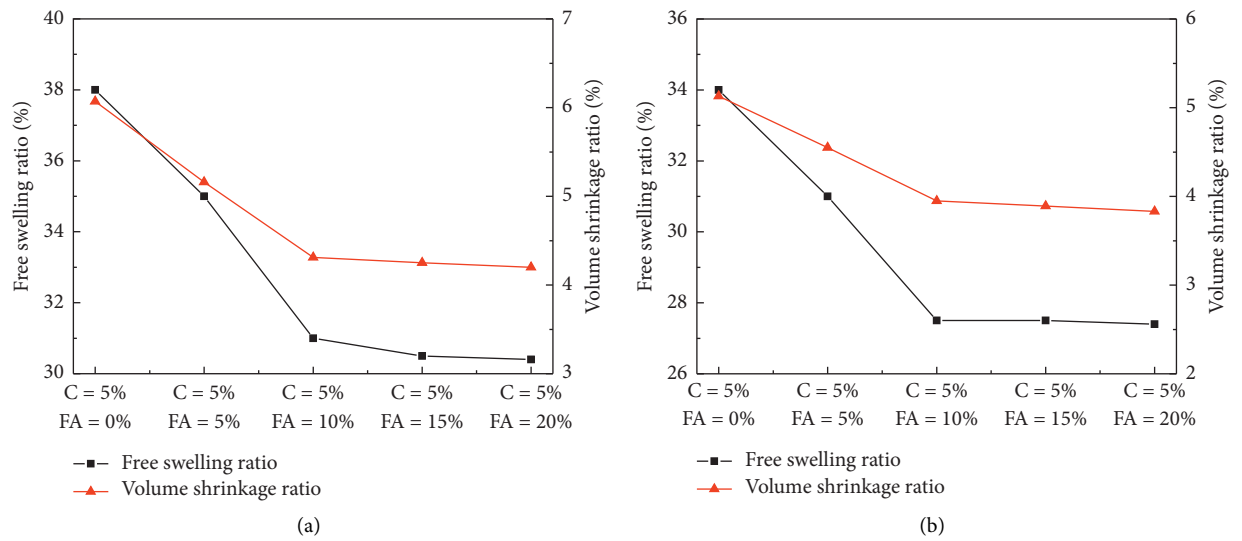

Figure 6: Swelling-shrinkage behaviors of cement-fly ash-stabilized soil under different curing periods. (a) 7 days. (b) 28 days.

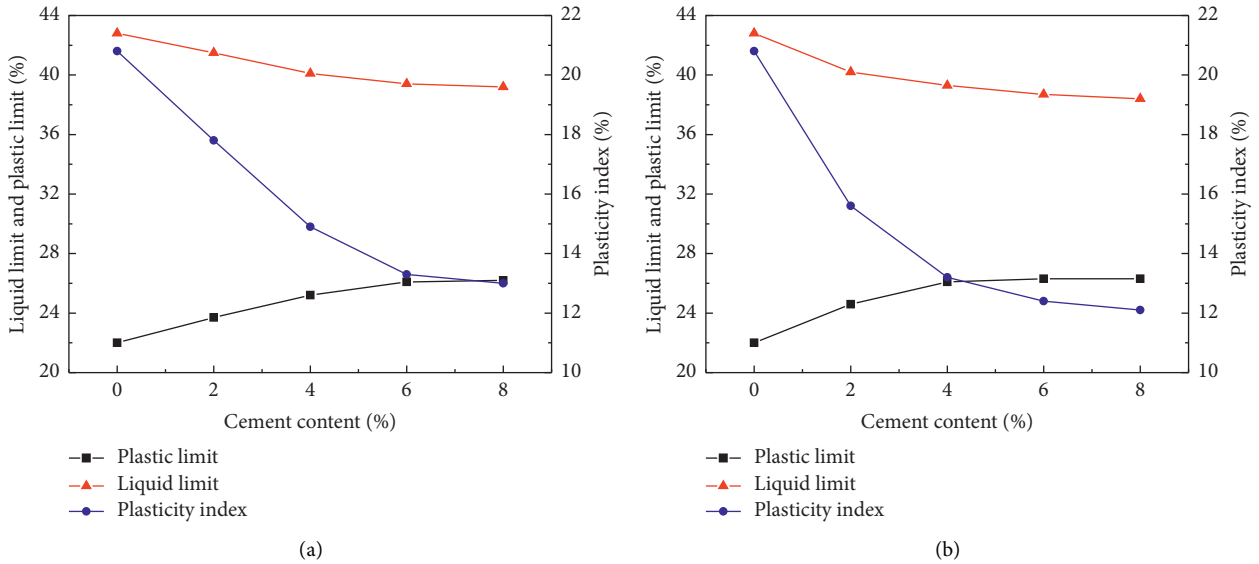

Figure 7: The Atterberg limits of cement-stabilized soil under different curing periods. (a) 7 days. (b) 28 days.

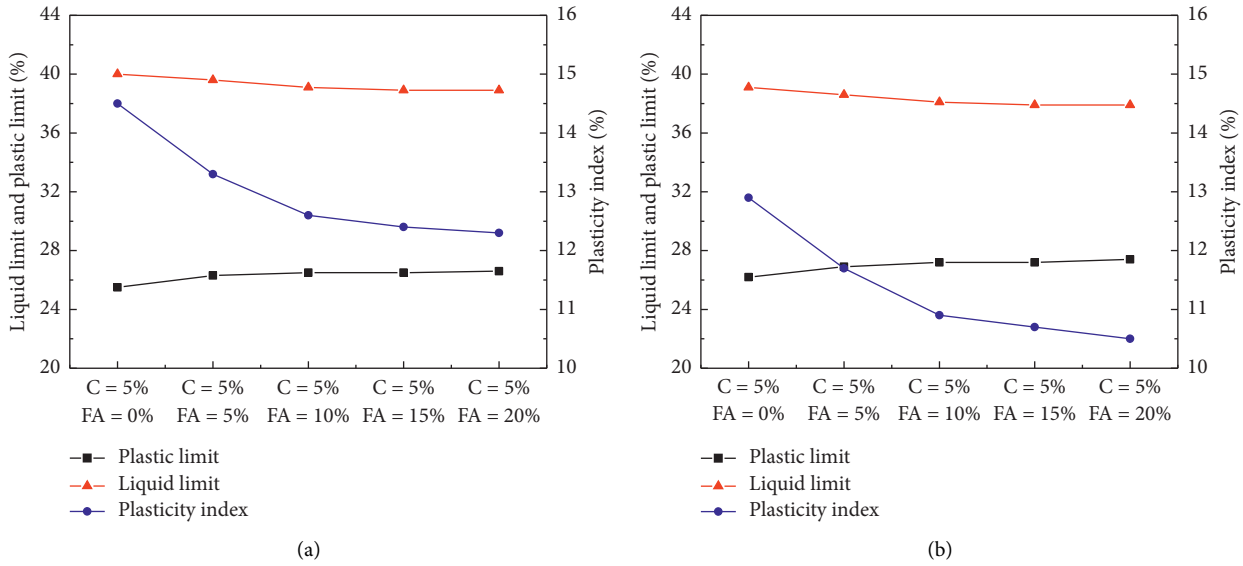

Figure 8: The Atterberg limits of cement-fly ash-stabilized soil under different curing periods. (a) 7 days. (b) 28 days.

a slight variation trend when the fly ash content is in the range of 10%~20%. It is well known that the plasticity index is an important indicator to evaluate the swelling potential of expansive soil [2, 21]. Therefore, the lower value of plasticity index indicated that the expansive soil with lower swelling behavior. The reduction of plasticity can be explained with the cation exchange reaction and the flocculation of clay particles [2, 4, 38]. The addition of chemical stabilizers such as fly ash and cement may cause the happening of cation exchange process and flocculation reaction inside stabilized soil, which can make the internal structure of soil specimen more aggregated and flocculated [2]. Moreover, it can be seen in Figures 5–8 that the free swelling ratio, volume shrinkage ratio, and plasticity index of stabilized soil with 5% cement and 10% fly ash is similar to the stabilized soil with 8% cement. Consequently, the stabilization of cement and fly ash can produce a same result with the single stabilization of cement.

As shown in Figure 9, with the certain cement content (C) of 5%, the unconfined compressive strength of cement-fly ash-stabilized soil increases at first and then decreases as the fly ash content (FA) increases from 0% to 20%. The inclusion of 5% or 10% fly ash into stabilized soil with 5% cement improves the unconfined compressive strength of stabilized soil. When the fly ash content increases to 15% or 20%, the unconfined compressive strength exhibits a decreasing trend compared with the stabilized soil sample with 5% cement and 10% fly ash. With the inclusion of fly ash into stabilized soil, the pozzolanic reactions and the occurrence of flocculation are the main reasons to improve unconfined compressive strength of stabilized soil [9, 38]. Thus, the unconfined compressive strength of stabilized soil significantly enhanced with the fly ash content of 10%. However, because fly ash itself has no cohesion [9], the unreacted fly ash particles remained inside the soil structure directly caused the reduction in cohesive force among particles [38]. Consequently, the unconfined compressive strength of

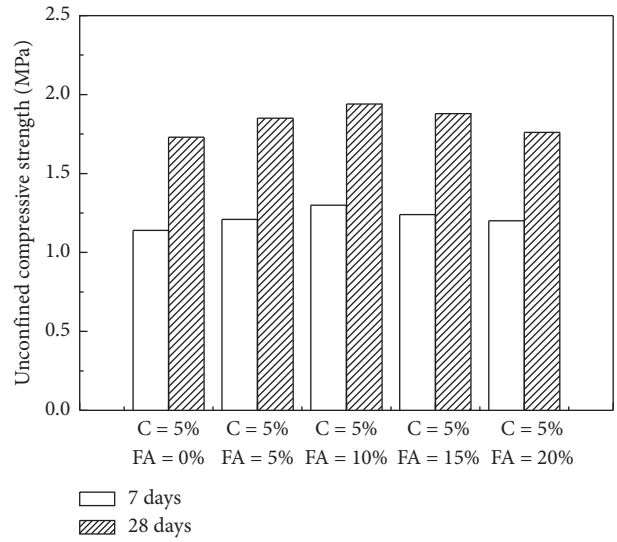

Figure 9: Unconfined compressive strength of cement-fly ash-stabilized soil.

stabilized soil showed a downward trend under the experimental condition of excess fly ash content (FA = 15% or FA = 20%). It is easily observed that the stabilized soil specimen with 5% cement and 10% fly ash shows an enhancement in unconfined compressive strength compared with stabilized soil specimen with 5% cement. When the mixtures are cured for 7 and 28 days, the maximum unconfined compressive strengths of cement-fly ash-stabilized soil (C = 5% and FA = 10%) are 1.30 MPa and 1.94 MPa, respectively. It can be concluded that the optimum mixed contents of cement and fly ash were regarded as 5% and 10%, respectively, according to the experimental results of physical and mechanical tests, which include swelling-shrinkage behaviors, plasticity index, and unconfined compressive strength.

3.2. Static Mechanical Properties of Basalt Fiber-Reinforced Cement-Fly Ash-Stabilized Soil

3.2.1. Static Stress-Strain Curves. Based on the findings of swelling-shrinkage behaviors, Atterberg limits, and unconfined compression tests, the cement content of 5% and fly ash content of 10% were applied in the following study of the static mechanical properties of basalt fiber-reinforced cement-fly ash-stabilized soil. For next investigation, the influence of basalt fiber content (BF) on static mechanical behaviors of cement-fly ash-stabilized soil is studied by unconfined compression tests. Figure 10 clearly shows the static stress-strain curves of cement-fly ash-stabilized soil under various basalt fiber contents. All the static stress-strain curves can be divided into three ordinal phases: elastic deformation phase, plastic deformation phase, and failure phase. For the first phase of elastic deformation, it can be seen that static stress of stabilized soil increases approximately in a line with an increase in the strain. Next, during the plastic deformation phase, the static stress presents a relative slow growth rate with the increase in strain. In the last phase, the static stress decreases obviously after the static stress reaches its peak value, namely, failure phase. Furthermore, the peak stress of stress-strain curve shows a notable upward trend when the basalt fiber content increased from 0% to 0.6%, and then appears a decreasing trend with the basalt fiber contents range from 0.9% to 1.2%. The peak strain of stress-strain curve also has a similar change trend with the peak stress. The basalt fiber-reinforced cement-fly ash-stabilized soil exhibits an optimal fiber content of 0.6% with maximum peak stress and peak strain. It can be concluded that the inclusion of basalt fiber into stabilized soil can effectively improve the ductility and constrain the deformation of cement-fly ash-stabilized soil [27, 39]. All the brittle characteristics of cement-fly ash-stabilized soil were modified due to the appearance of fiber reinforcement. With the addition of basalt fiber, the frictional force and bite force among soil particles enhanced significantly due to the generation of a three-dimensional internal space structure [40]. The failure mode of stabilized soil has transformed from brittle failure to plastic failure because of the combined actions of frictional force among soil particles and tensile force of fibers [39, 40]. Therefore, the corresponding stress and strain increase gradually when the fiber content increased from 0% to 0.6%. When the fiber content exceeds 0.6%, the excess fibers cannot present a uniform distributed state inside the stabilized soil. The occurrence of fiber accumulation directly causes the damage of three-dimensional internal space structure [40]. Accordingly, the corresponding stress and strain show a decreasing trend under the fiber contents of 0.9% and 1.2%.

3.2.2. Unconfined Compressive Strength. The unconfined compressive strength refers to the peak stress in the static stress-strain curve. As shown in Figure 11, the unconfined compressive strength of cement-fly ash-stabilized soil increases first and decreases subsequently with the basalt fiber content varying in the range of 0% to 1.2%. With the basalt fiber content of 0.6%, the average value of unconfined compressive strength reaches its maximum value of 2.36 MPa. Under the basalt fiber content of 0.6%, the basalt fiber-reinforced cement-fly ash-stabilized soil provides a desirable mechanical performance than cement-fly ash-stabilized soil with 0% basalt fiber. Moreover, the unconfined compressive strength tends to decrease with fiber contents from 0.6% to 1.2%. When the basalt fiber content is 1.2%, the unconfined compressive strength has a notable reduction compared with the basalt fiber content of 0.6%. The cement-fly ash-stabilized soil reinforced with 0.6% basalt fiber has a remarkable improvement in unconfined compressive strength because of the fiber bridging capacity and the formation of stable space structure inside stabilized soil [27, 39, 40]. However, the alleviation of fiber bridging effect and the breakage of stable three-dimensional space structure owing to the addition of excess basalt fibers to stabilized soil [27, 40].

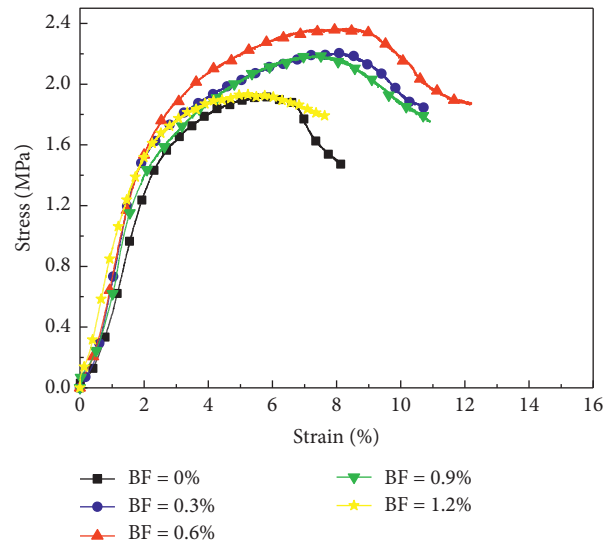

Figure 10: Static stress-strain curves of basalt fiber-reinforced cement-fly ash-stabilized soil.

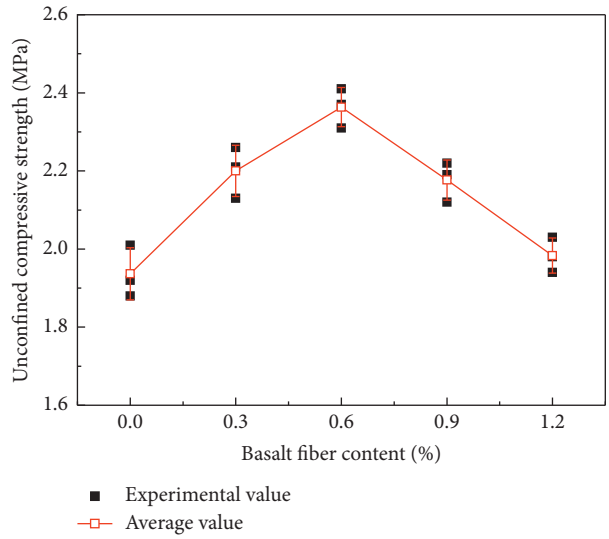

Figure 11: Unconfined compressive strength of basalt fiber-reinforced cement-fly ash-stabilized soil.

3.3. Dynamic Mechanical Properties of Basalt Fiber-Reinforced Cement-Fly Ash-Stabilized Soil

3.3.1. Dynamic Stress-Strain Curves. The dynamic compression tests of basalt fiber-reinforced cement-fly ash-stabilized soil were performed according to the optimum mixed contents of cement and fly ash. According to one-dimensional wave theory, the dynamic stress, strain, and strain rate histories of stabilized soil can be determined by the corresponding equations in [41]. Thus, the dynamic stress-strain curves of cement-fly ash-stabilized soil under different basalt fiber dosages and impact loading pressures were obtained and presented in Figure 12. The dynamic stress increases with increasing strain until the dynamic stress obtains its peak value. Thereafter, the dynamic stress decreases significantly as the strain increased to ultimate strain. For cement-fly ash-stabilized soil with 0.6% basalt fiber, the dynamic stress reaches its maximum value at a given impact loading pressure. Similar to static stress-strain curve, the dynamic stress-strain curve can be divided into three phases, namely, approximate elastic deformation phase, plastic yield hardening deformation phase, and failure phase. The dynamic stress increases with strain by nearly linear approximation in the first phase. For the second phase, the dynamic stress increases slowly with the increase in strain. The stabilized soil specimen shows a plastic behavior in the second phase. For the failure phase, the dynamic stress decreases directly with a further increase in strain. The ultimate strain of cement-fly ash-stabilized soil does not change obviously with the variation of basalt fiber content. Nevertheless, the ultimate strain of cement-fly ash-stabilized soil increases correspondingly with increasing impact loading pressure. Besides, all the curves have a similar ultimate strain under the certain impact loading pressure, which considered as the strain convergence phenomenon of dynamic stress-strain curves. This phenomenon has not appeared in the static stress-strain curves.

3.3.2. Dynamic Compressive Strength. The peak stress value of dynamic stress-strain curves was named as dynamic compressive strength. As shown in Figure 13, there are two factors of basalt fiber content and impact loading pressure affecting the variation of dynamic compressive strength. For a same basalt fiber dosage, the dynamic compressive strength increases remarkably with an increase in impact loading pressure. For instance, the dynamic compressive strength of cement-fly ash-stabilized soil with 0.6% basalt fiber reaches 7.58 MPa at 0.5 MPa impact loading pressure, which has a growth rate of 46.62% compared with the experimental condition of 0.3 MPa impact loading pressure.

For each impact loading pressure, the dynamic compressive strength of cement-fly ash-stabilized soil increases first and then decreases with basalt fiber contents from 0% to 1.2%. This variation tendency is similar to the finding of previous research [27]. When the basalt fiber content of 0.6%, the dynamic compressive strength has a maximum enhancement compared with unreinforced cement-fly ash-stabilized soil. It is easily found that there is a significant reduction in dynamic compressive strength as the basalt fiber content exceeds its optimum content of 0.6%. This is an evidence to certify that the excess basalt fiber has a negative effect on the improvement of dynamic compressive strength. The enhancement in dynamic compressive strength can be explained by the following reasons: (1) with the addition of basalt fiber, the interfacial bonding strength between fiber and soil matrix is enhanced [42]; (2) the formation of fiber-hydration products-soil mixture provides a better adhesion among soil particles; (3) the stable three-dimensional fiber-soil net generated inside the stabilized soil due to the bridging capacity of basalt fiber [27, 42]; and (4) the good impact resistance of basalt fiber [27]. Therefore, the cement-fly ash-stabilized soil has a significant improvement in dynamic compressive strength with the inclusion of basalt fiber. With the basalt fiber contents from 0.6% to 1.2%, the dynamic compressive strength of stabilized soil drops obviously due to the existence of weak interfaces (namely, fiber-fiber accumulated interfaces) and the damage of stable three-dimensional space structure [27].

It is known that the dynamic mechanical properties of stabilized soil have an obvious difference with static mechanical properties. To obtain a better comparative analysis between dynamic compressive strength and static compressive strength, the dynamic increase factor (DIF) is a good indicator to measure the growth of dynamic strength [41]. Therefore, the dynamic increase factor is selected in the next analysis. The DIF can be calculated by the following equation:

$$\mathrm{DIF} = \frac{f_{\mathrm{d}}}{f_{\mathrm{s}}}, \tag{1}$$

where f_{d} stands for the dynamic compressive strength of basalt fiber-reinforced cement-fly ash-stabilized soil and f_{s} represents the static compressive strength (namely, unconfined compressive strength) under the same experimental condition (namely, the same basalt fiber content) with dynamic compression test.

As presented in Figure 14, the compressive strength of basalt fiber-reinforced cement-fly ash-stabilized soil under impact loading exhibits a conspicuous enhancement over static loading. Moreover, for each fiber dosage, there is a remarkable increasing trend between DIF and impact loading pressure. This phenomenon can be explained from two aspects. First, the stabilized soil specimen transformed from the uniaxial stress state into the uniaxial strain state due to the increasing impact loading pressure. The significant improvement in DIF is a result of the lateral confinement. Because the lateral confinement is more obvious under high strain rate, the strength of stabilized soil shows a sharp upward trend [27]. Next, the impact loading time is very short when compared with static loading time. Therefore, there are many new microcracks generated inside stabilized soil before the final failure of stabilized soil under impact loading, which would consume more energy and result in higher dynamic strength [41].

3.3.3. Energy Absorption Properties. The energy absorption characteristics of stabilized soil under impact loading are beneficial to reflect the intrinsic mechanism of the

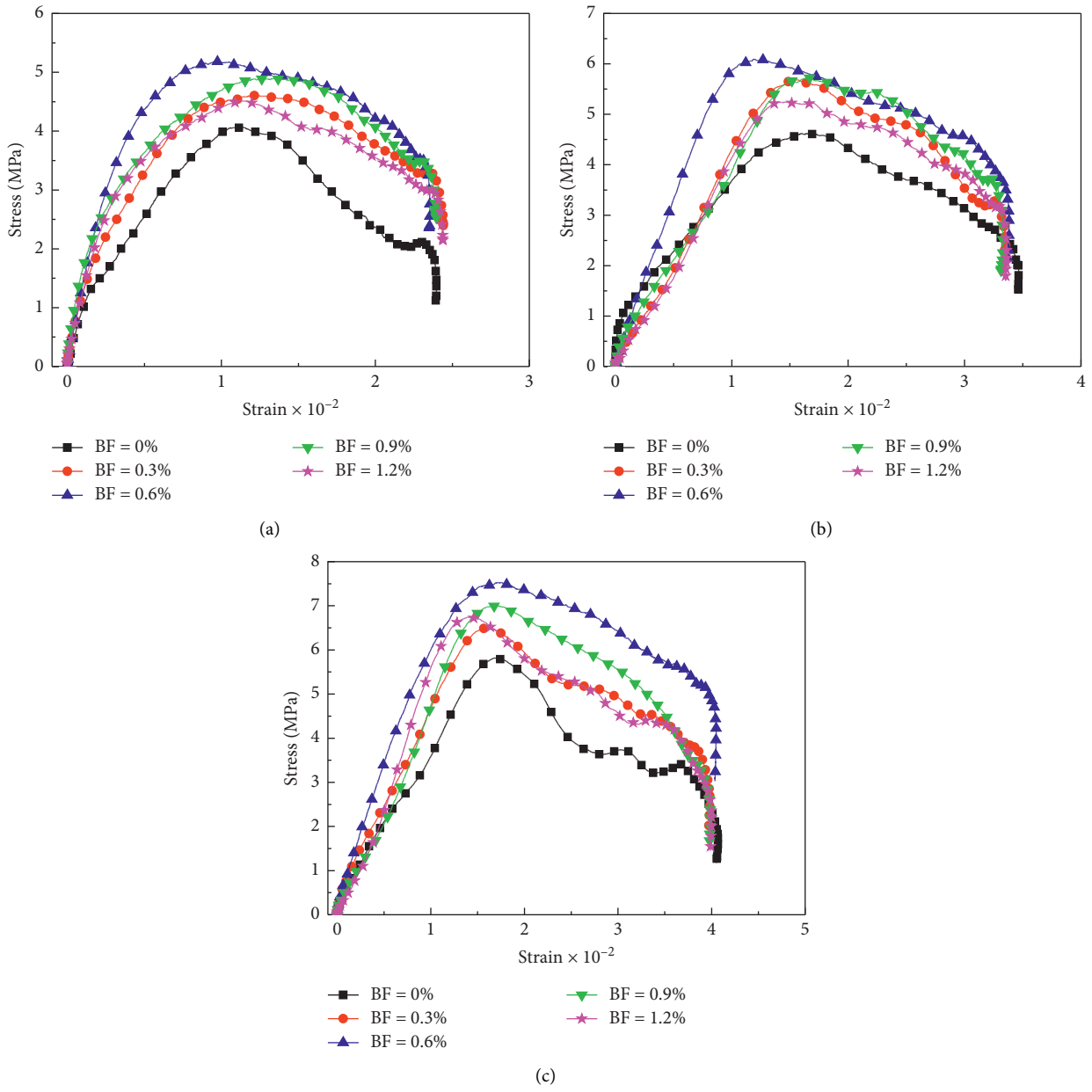

Figure 12: Dynamic stress-strain curves of basalt fiber-reinforced cement-fly ash-stabilized soil. (a) 0.3 MPa impact loading pressure. (b) 0.4 MPa impact loading pressure. (c) 0.5 MPa impact loading pressure.

macroscopic final failure of stabilized soil. During the dynamic compression tests (namely, SHPB tests), the involved energies are composed of incident energy, reflected energy, transmitted energy, and absorbed energy of stabilized soil sample. The calculated equations for incident energy, reflected energy, and transmitted energy are as follows:

$$\begin{cases} W_{\mathrm{I}} = \mathrm{EAC} \int \varepsilon_{\mathrm{I}}^2(t)\mathrm{d}t, \\ W_{\mathrm{R}} = \mathrm{EAC} \int \varepsilon_{\mathrm{R}}^2(t)\mathrm{d}t, \\ W_{\mathrm{T}} = \mathrm{EAC} \int \varepsilon_{\mathrm{T}}^2(t)\mathrm{d}t, \end{cases} \tag{2}$$

where W_{I}, W_{R}, and W_{T} are the incident energy, reflected energy, and transmitted energy, respectively; $\varepsilon_{\mathrm{I}}(t)$, $\varepsilon_{\mathrm{R}}(t)$, and $\varepsilon_{\mathrm{T}}(t)$ stand for the incident, reflected, and transmitted strain signals measured, respectively.

In SHPB tests, the energy loss caused by the friction effect can be ignored due to the application of lubricant, the absorbed energy (W_{S}) of the stabilized soil specimen can be calculated as follows:

$$W_{\mathrm{S}} = W_{\mathrm{I}} - W_{\mathrm{R}} - W_{\mathrm{T}}. \tag{3}$$

On the basis of the SHPB experiment data, the absorbed energy of the stabilized soil sample can be calculated according to the aforementioned equations and the results of calculation are shown in Figure 15.

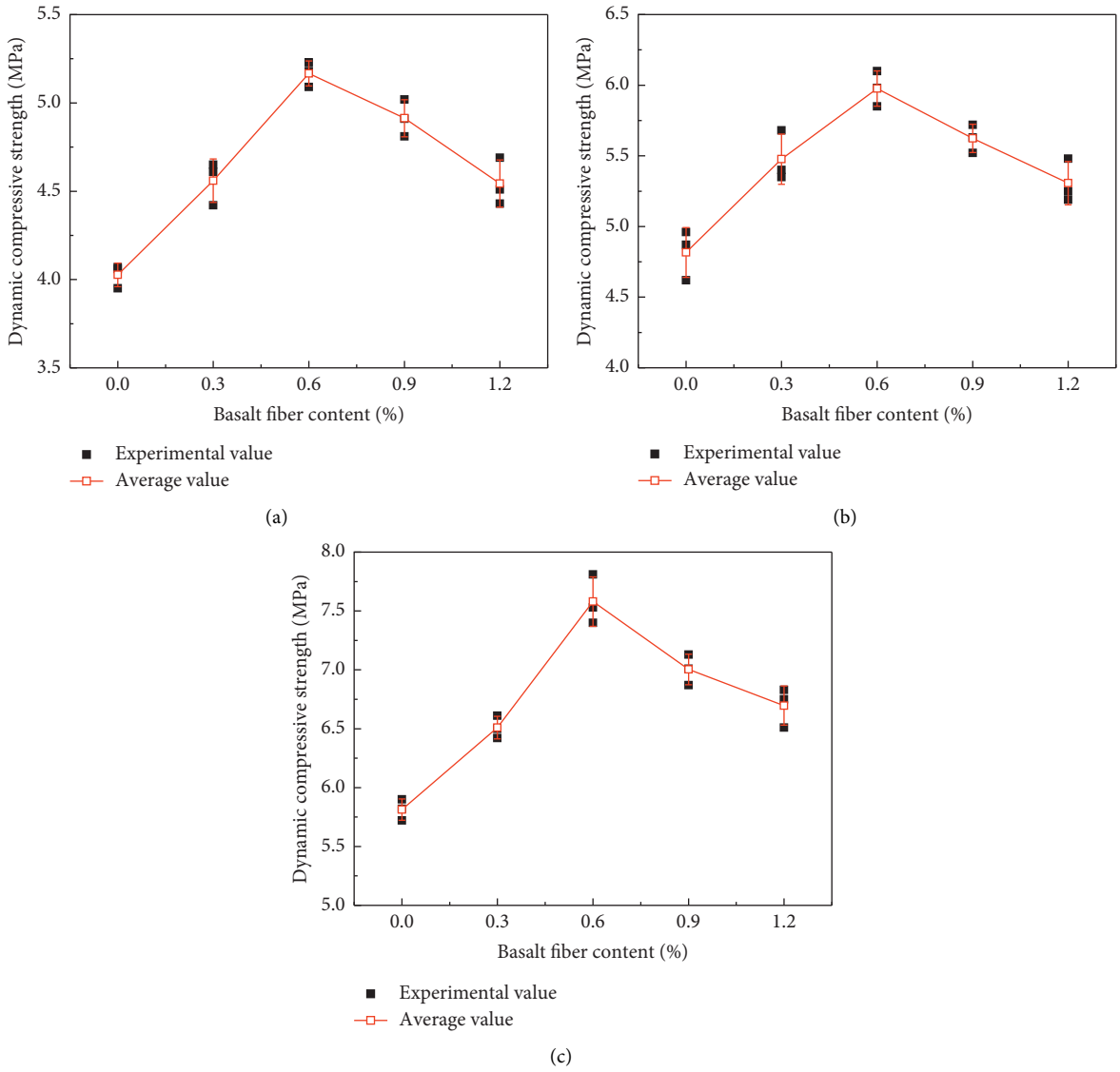

Figure 13: Dynamic compressive strength of basalt fiber-reinforced cement-fly ash-stabilized soil. (a) 0.3 MPa impact loading pressure. (b) 0.4 MPa impact loading pressure. (c) 0.5 MPa impact loading pressure.

The variation curves of energy versus time are presented in Figure 15. At the same basalt fiber content and impact loading pressure, it can be seen that the absorbed energy increases slowly with the time growing at initial phase. Subsequently, the absorbed energy increases in a relatively rapid way. At last, the absorbed energy increases slowly again and keeps at a stable value. Besides, at the same basalt fiber dosage, the absorbed energy of stabilized soil specimen presents an increasing trend with the increase in impact loading pressure. The bigger the impact loading pressure, the larger the incident energy, so the absorbed energy has a significant improvement. For the same impact loading pressure, the addition of basalt fiber into cement-fly ash-stabilized soil can make a big contribution to the enhancement of energy absorption ability.

To analyze the energy absorption characteristics of stabilized soil specimen more accurately, the specific energy absorption (SEA) can be introduced in this study. SEA represents the energy absorption of specimen per unit volume, and it can be calculated as follows:

$$\mathrm{SEA} = \frac{W_S}{A_s l_s}, \tag{4}$$

where A_s and l_s are the cross-sectional area and original length of stabilized soil specimen, respectively.

Figure 16 presents the relationship between specific energy absorption (SEA) and basalt fiber content. Under the same impact loading pressure, it can be easily found from Figure 16 that the specific energy absorption of stabilized soil increases first and decreases subsequently with increasing basalt fiber content. The specific energy absorption increases significantly with basalt fiber contents from 0% to 0.6%. The cement-fly ash-stabilized soil with 0.6% basalt fiber reached its maximum value in specific energy absorption. After that, the specific energy absorption decreases gradually with basalt fiber contents from 0.6% to 1.2%. Because the basalt

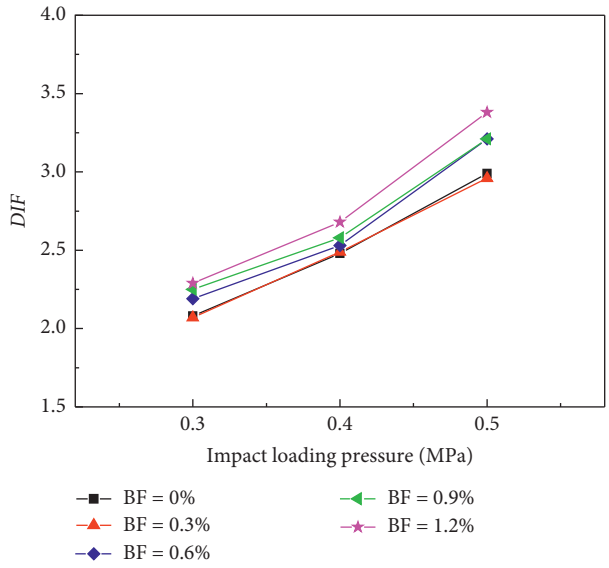

Figure 14: Dynamic increase factor of stabilized soil.

fiber plays an important role in reinforcement and prevention of crack development, the inclusion of basalt fiber can improve the integrality of internal structure of cement-fly ash-stabilized soil. With the basalt fiber content of 0.6%, a stable three-dimensional space structure formed inside stabilized soil by the connection and interaction of randomly distributed fibers, cementitious products, and soil particles [27, 39]. When the stabilized soil is subjected to impact loading, the pull-out failure occurs due to the insufficient adhesion and connection between fibers and interfaces of stabilized soil. A large number of new microcracks generated and extended inside stabilized soil during the pull-out process of basalt fibers. Therefore, the specific energy absorption of cement-fly ash-stabilized soil with 0.6% basalt fiber shows a maximum enhancement. However, more fiber-fiber accumulated interfaces occurred inside stabilized soil with the further inclusion of basalt fiber [27]. With the basalt fiber contents of 0.9% and 1.2%, it can be seen that many fiber accumulation phenomena appeared inside the stabilized soil in the later microstructure analysis. The fiber-fiber weak interfaces directly result in sliding failure as the stabilized soil is subjected to impact loading. Accordingly, the specific energy absorption decreases gradually when the basalt fiber content increased from 0.6% to 1.2%. In addition, the specific energy absorption of stabilized soil increases remarkably with the increase in impact loading pressure.

3.3.4. Failure Pattern. The failure patterns of cement-fly ash-stabilized soil under various basalt fiber contents and impact loading pressures are shown in Figure 17. For the same impact loading pressure, the amount of broken fragments decreases with an increase in basalt fiber content and the size of broken fragments increases with increasing basalt fiber content. As a consequence, the addition of basalt fiber can change the failure pattern of stabilized soil under impact loading. With the increase in impact loading pressure, the size of broken fragments notably decreases and the amount of broken fragments significantly increases. The shape of broken fragments transformed from large blocks into crushed pieces with the impact loading pressure increased from 0.3 MPa to 0.5 MPa.

3.3.5. Fractal Characteristics. Fractal geometry can be used to study the irregularity, self-similarity, and complexity of objects (such as broken fragments generated in SHPB tests). The sieving tests were performed to research the fractal characteristics of broken fragments. In sieving tests, 10 kinds of standard sieves were adopted in this study, namely, 0~0.15 mm, 0.15~0.3 mm, 0.3~0.6 mm, 0.6~1.18 mm, 1.18~2.36 mm, 2.36~4.75 mm, 4.75~9.5 mm, 9.5~16 mm, 16~26.5 mm, and 26.5~31.5 mm standard sieves. The machine shaking was applied in sieving tests for purpose of reducing experimental errors. The shaking time was fixed at 2 minutes. After that, the weight of broken fragments remained in each grade standard sieve was measured with high-sensitivity electronic scale.

As shown in Tables 3–5, the size distribution of broken fragments changes gradually with the increase in basalt fiber content. At a constant impact loading pressure, the quantities of large-size fragments show an increasing trend and the quantities of small-size fragments present a decreasing trend with an increase in basalt content. Furthermore, the impact loading pressure can also change the size distribution of broken fragments. With the increase in impact loading pressure, the number of large-size fragments decreases correspondingly and the number of small-size fragments increases significantly.

The fractal dimension can directly reflect the degree of fragmentation of stabilized soil under impact loading; thus, the fractal characteristics of impact broken fragments are analyzed by fractal dimension. The calculation of fractal dimension is based on the G-G-S distribution function model [43] and the mass-frequency relationship [44], and the ratio of partial mass to the total mass can be acquired by the following equation:

$$Y = \frac{M_r}{M_T} = \left(\frac{r}{r_m}\right)^b, \tag{5}$$

where M_r stands for the cumulative mass of fragments with the particle size less than r and M_T stands for total mass of fragments, r is the size of fragments and r_m is maximum size of fragments, and b represents a distribution parameter.

The fractal dimension (D_b) is dependent on the size of fragments (r) and the amount of fragments (N) with a particle size larger than r. The relationship among these three parameters can be described by the following equation:

$$N = r^{-D_b}. \tag{6}$$

The relationship between the increment in the number of broken fragments and the increment in the mass of broken fragments can be described by $dM \infty r^3 dN$. The fractal dimension satisfied the equation of $D_b = 3-b$. The $(3-D_b)$ can be considered as the slope of fitting line in the coordinate frame of $\ln(M_r/M_T)$-$\ln r$.

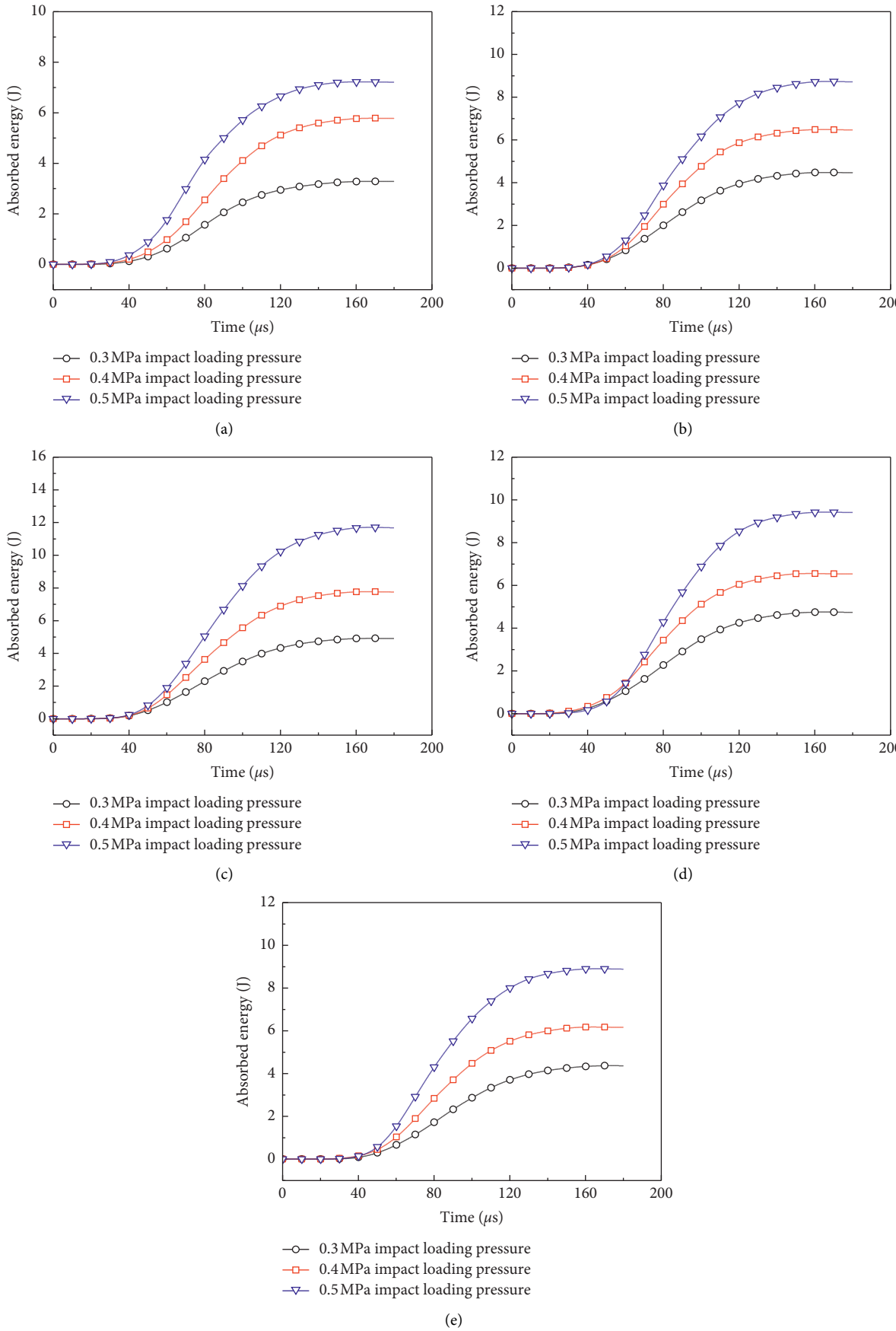

Figure 15: Curves of energy versus time for basalt fiber-reinforced cement-fly ash-stabilized soil. (a) BF = 0%. (b) BF = 0.3%. (c) BF = 0.6%. (d) BF = 0.9%. (e) BF = 1.2%.

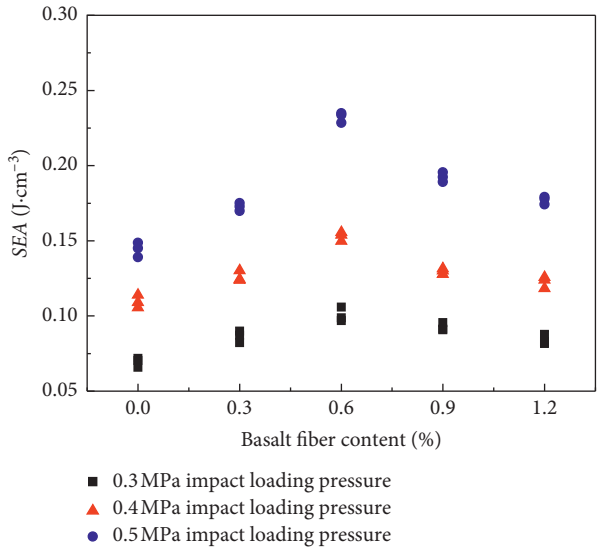

Figure 16: Relationship between specific energy absorption and basalt fiber content.

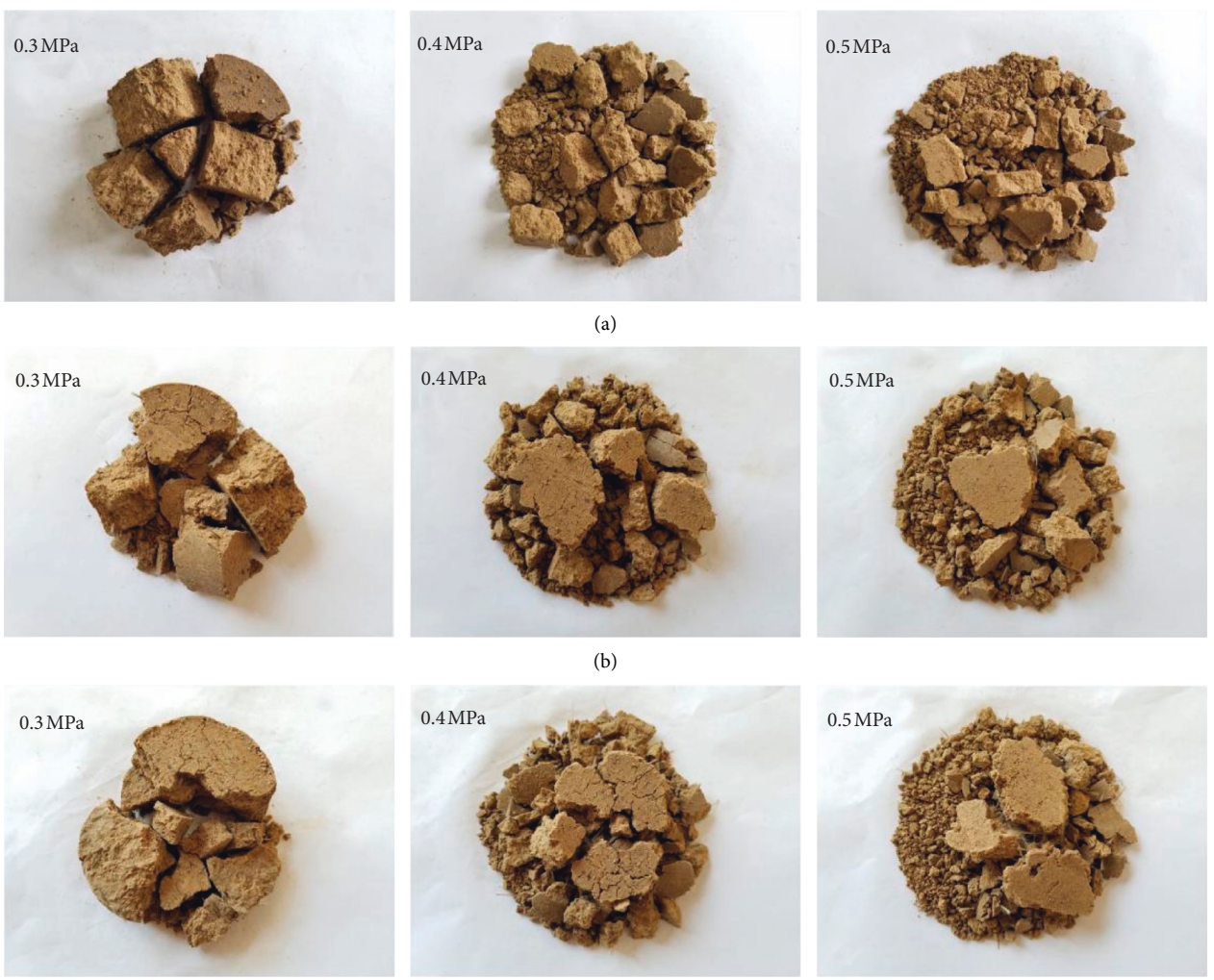

Figure 17: Continued.

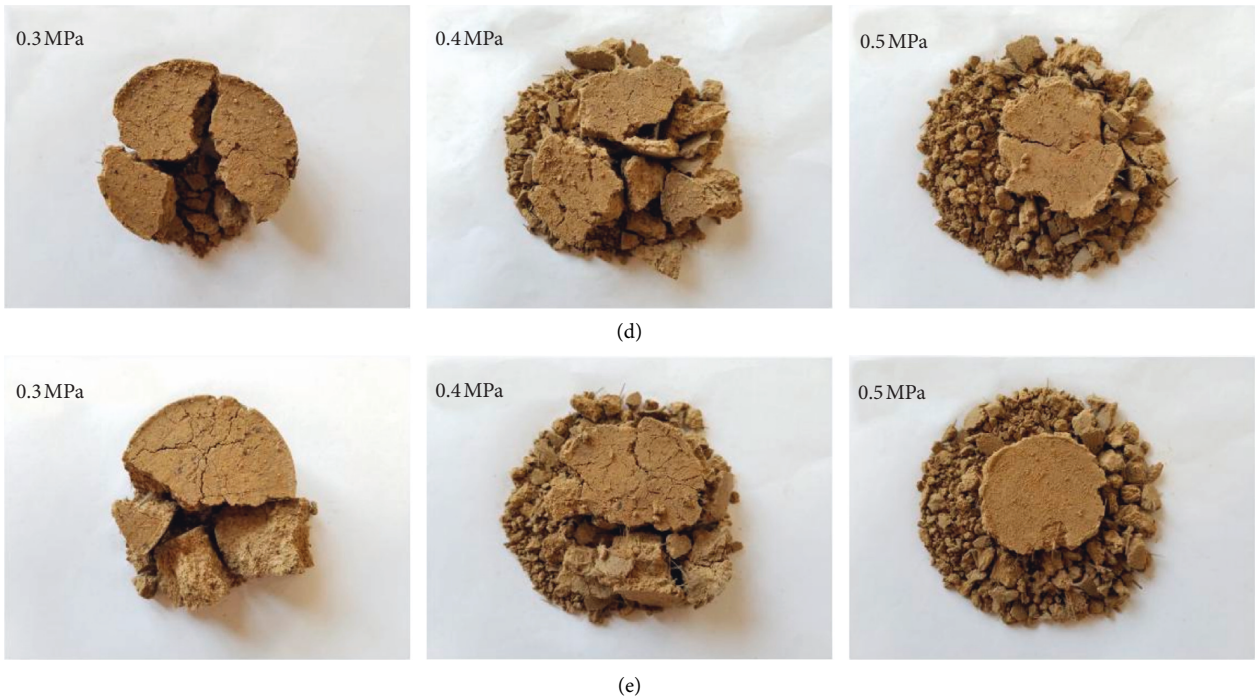

Figure 17: Failure patterns of basalt fiber-reinforced cement-fly ash-stabilized soil in SHPB tests. (a) BF = 0%. (b) BF = 0.3%. (c) BF = 0.6%. (d) BF = 0.9%. (e) BF = 1.2%.

Table 3: Sieving test results of impact fragments of basalt fiber-reinforced cement-fly ash-stabilized soil (0.3 MPa impact loading pressure).

BF (%)	Mesh size (mm)										Total mass (g)
	0	0.15	0.3	0.6	1.18	2.36	4.75	9.5	16	26.5	
0	0.20	0.19	0.36	0.63	0.95	2.54	4.20	21.34	32.25	24.75	87.41
0.3	0.18	0.16	0.32	0.62	0.88	2.33	4.52	18.82	33.20	25.93	86.96
0.6	0.13	0.14	0.31	0.52	0.71	2.04	2.05	16.22	36.56	28.05	86.73
0.9	0.11	0.12	0.29	0.45	0.63	1.33	2.09	14.27	36.34	32.24	87.87
1.2	0.09	0.11	0.26	0.41	0.56	1.29	2.06	9.76	35.44	37.11	87.09

Table 4: Sieving test results of impact fragments of basalt fiber-reinforced cement-fly ash-stabilized soil (0.4 MPa impact loading pressure).

BF (%)	Mesh size (mm)										Total mass (g)
	0	0.15	0.3	0.6	1.18	2.36	4.75	9.5	16	26.5	
0	0.80	0.95	2.05	3.10	5.67	5.41	6.98	16.01	29.73	16.81	87.51
0.3	0.71	0.84	1.76	2.97	5.09	5.38	6.21	13.12	30.29	21.66	88.03
0.6	0.59	0.73	1.54	2.54	4.53	4.02	4.88	10.28	33.53	24.34	86.98
0.9	0.51	0.59	1.29	2.13	4.49	4.04	4.67	6.35	34.66	28.95	87.68
1.2	0.43	0.49	1.18	1.87	4.29	3.89	4.45	5.81	30.04	34.76	87.21

Table 5: Sieving test results of impact fragments of basalt fiber-reinforced cement-fly ash-stabilized soil (0.5 MPa impact loading pressure).

BF (%)	Mesh size (mm)										Total mass (g)
	0	0.15	0.3	0.6	1.18	2.36	4.75	9.5	16	26.5	
0	2.07	2.03	2.17	3.49	4.58	8.77	7.95	24.46	31.78	0	87.30
0.3	1.32	2.21	2.73	4.31	5.06	9.32	10.69	15.60	23.31	13.11	87.66
0.6	1.15	1.73	2.24	3.29	4.54	9.28	9.75	10.25	25.97	18.69	86.89
0.9	1.05	1.31	1.82	2.36	4.01	8.79	10.09	12.72	22.05	22.88	87.08
1.2	1.07	1.17	1.66	2.25	3.97	8.35	12.47	12.62	16.82	27.54	87.92

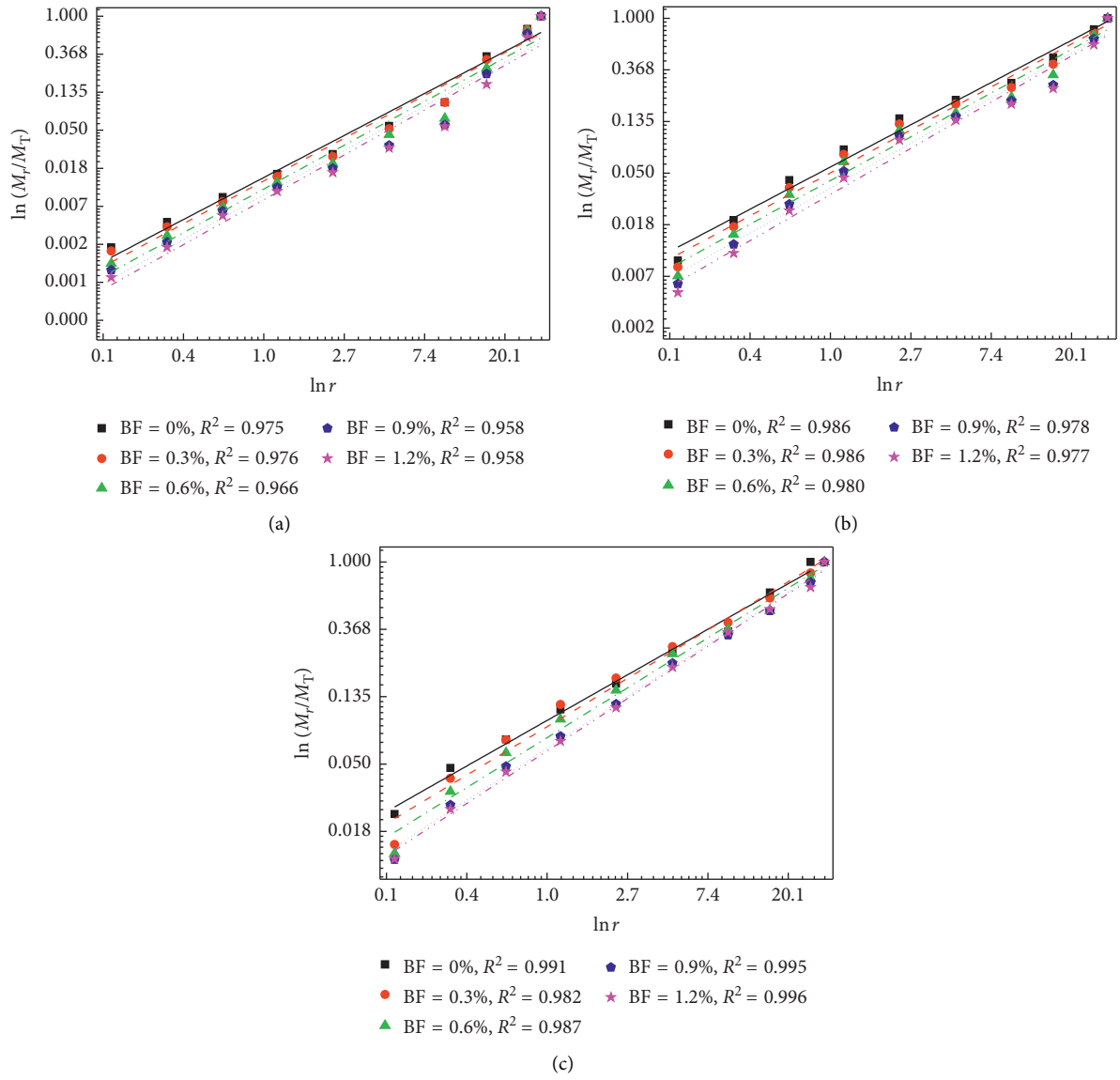

FIGURE 18: Diagrams of $\ln(M_r/M_T)$-$\ln r$ curves. (a) 0.3 MPa impact loading pressure. (b) 0.4 MPa impact loading pressure. (c) 0.5 MPa impact loading pressure.

Under different impact loading pressures and basalt fiber contents, the correlation coefficients of the fitting straight lines presented in Figure 18 are above 0.95. Accordingly, the broken fragments of stabilized soil display the fractal characteristic and self-similarity.

The relationship between fractal dimension and basalt fiber content is exhibited in Figure 19. Under the impact loading pressure of 0.3 MPa, the fractal dimension gradually decreases from 1.89 to 1.81 with the increase in basalt fiber content. Similarly, at the 0.4 MPa and 0.5 MPa impact loading pressures, the fractal dimension values, respectively, decrease from 2.19 to 2.10 and 2.32 to 2.21 with increasing fiber content. In contrast to unreinforced cement-fly ash-stabilized soil, the average fractal dimension values of cement-fly ash-stabilized soil with 1.2% basalt fiber are, respectively, reduced by 3.19%, 3.21%, and 3.90% under the impact loading pressures of 0.3 MPa, 0.4 MPa, and 0.5 MPa. It can be deduced that the addition of basalt fiber can change the fractal dimension of impact fragments and the fragmentation degree of stabilized soil.

3.4. Microstructure Analysis of Basalt Fiber-Reinforced Cement-Fly Ash-Stabilized Soil. Attempts have been done in the foregoing sections to investigate the effects of basalt fiber content on static stress-strain curves, unconfined compressive strength, dynamic stress-strain curves, dynamic compressive strength, energy absorption, failure modes, and fractal characteristics of cement-fly ash-stabilized soil. In the next section, the microstructural studies were carried out to make an explanation for the inner mechanism of macroscopic behaviors.

Figure 20 shows the basalt fiber surface inside cement-fly ash-stabilized soil. It is easily seen that the basalt fiber can fill

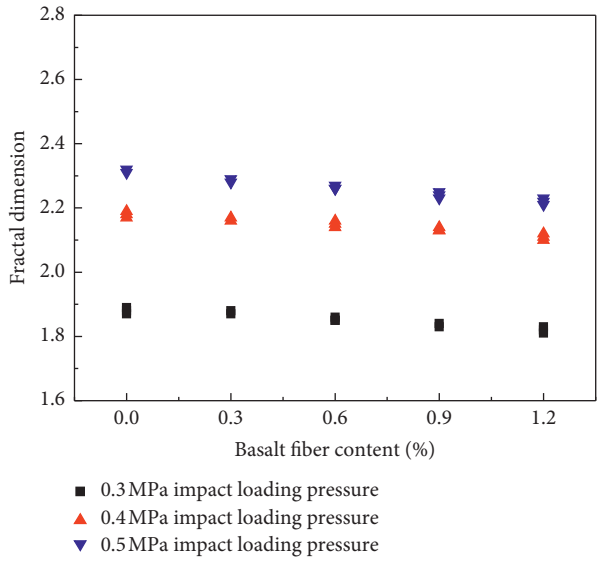

Figure 19: Relationship between fractal dimension and basalt fiber content.

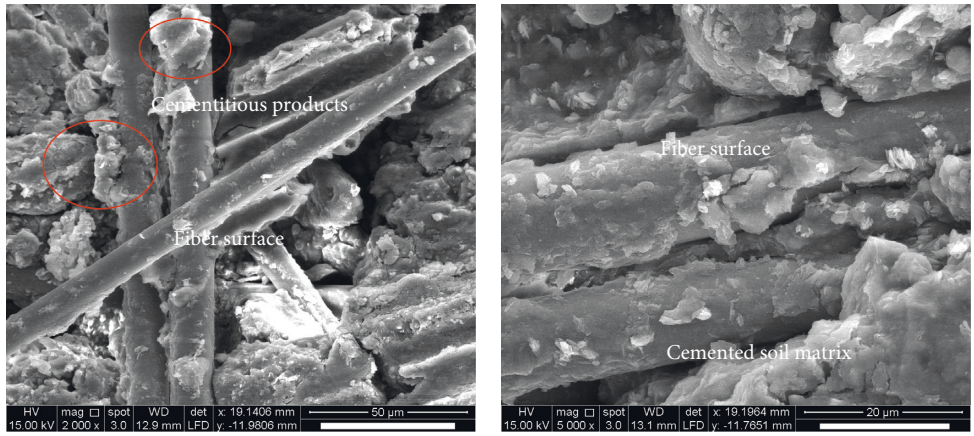

(a) (b)

Figure 20: SEM images of the basalt fiber surface inside cement-fly ash-stabilized soil. (a) 2000x. (b) 5000x.

the micropores among soil particles and aggregations. As shown in Figure 20(a), the presence of cementitious products on the surfaces of basalt fibers is a reason of the significant improvement in bonding strength and interfacial force [27, 39]. With a higher magnification exhibited in Figure 20(b), it can be seen that there are so many cementitious products that almost completely adhere on the main areas of fiber surface. Besides, it can be observed that the part of basalt fiber was tightly embedded into cemented soil matrix in Figure 20(b). The SEM observation of basalt fiber surface can become a good interpretation to support the macroscopic mechanical properties.

The alteration of the microstructure of cement-fly ash-stabilized soil under different basalt fiber contents is clearly presented in Figure 21. Compared with the stabilized soil specimens reinforced with basalt fiber, an uncompacted internal structure of unreinforced stabilized soil is presented in Figure 21(a). As shown in Figure 21(b), the addition of basalt fibers is capable of improving the connection among soil particles and the integrality of internal structure. It can be observed that the basalt fibers were closely surrounded by soil particles, soil matrix, and cementitious products in Figure 21(c). With the basalt fiber content of 0.6%, the randomly distributed basalt fibers and cemented soil matrix interact with each other and generate a stable internal space structure [27, 42]. Consequently, the macroscale mechanical behaviors presented in previous sections have a maximum improvement of cement-fly ash-stabilized soil with 0.6% basalt fiber, which include the enhancements of static compressive strength, dynamic compressive strength, and energy absorption capacity. With the basalt fiber contents of 0.9% and 1.2%, it is easily found from Figures 21(d) and 21(e) that the accumulated and overlapped phenomena of fibers occurred inside stabilized soil. The accumulation of basalt fibers is very evident in Figure 21(e), which exhibits many fiber-fiber accumulated interfaces. Because the fiber-fiber

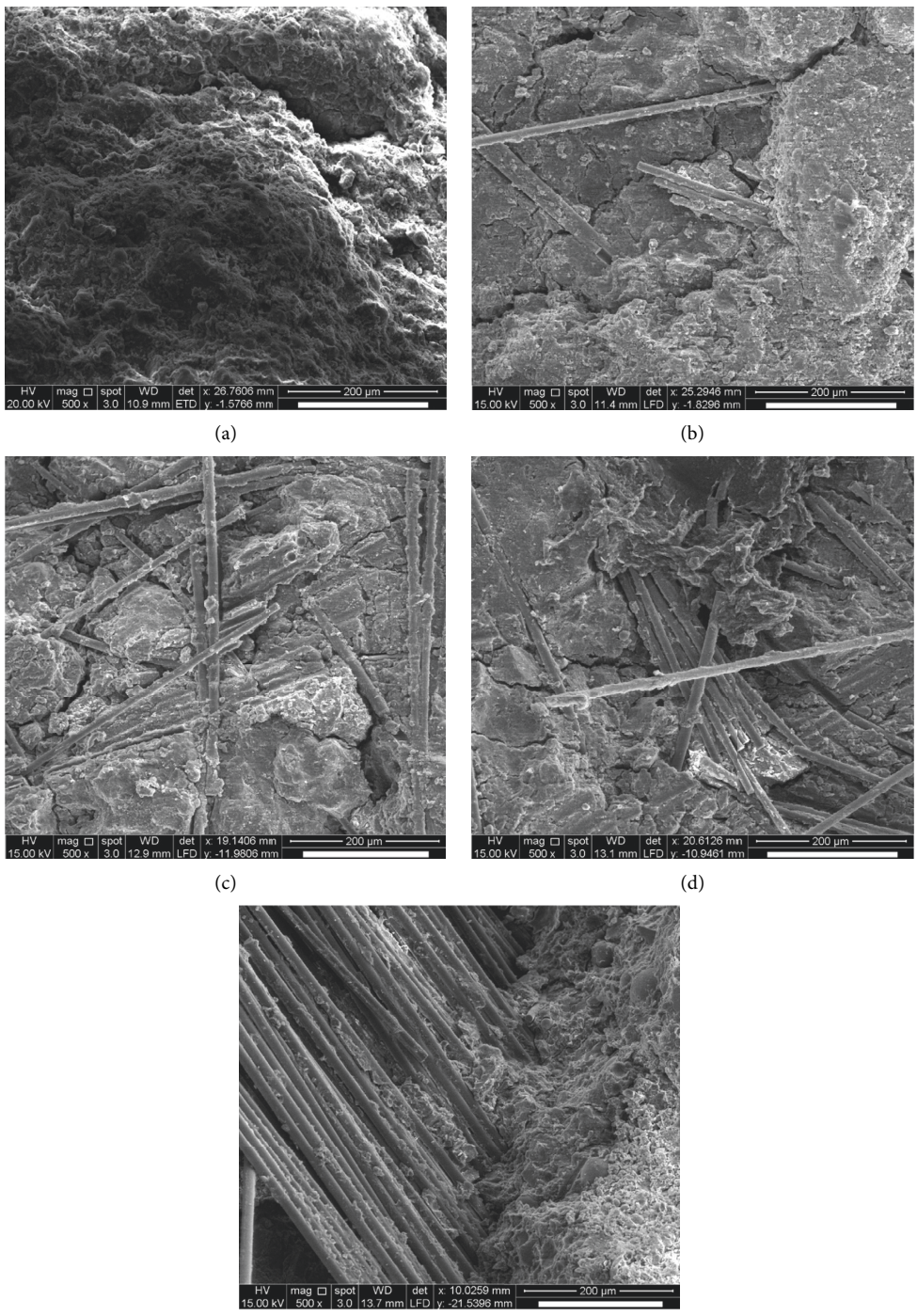

Figure 21: SEM images of cement-fly ash-stabilized soil with different basalt fiber contents. (a) BF = 0%. (b) BF = 0.3%. (c) BF = 0.6%. (d) BF = 0.9%. (e) BF = 1.2%.

accumulated interfaces are regarded as the weak interfaces, the stabilized soil directly generates the sliding failure under external loading [27]. Therefore, the static-dynamic mechanical properties show a notable downward trend with the basalt fiber content of 1.2%. The large fragments can be seen with the naked eye in the failure pattern of cement-fly ash-stabilized soil with 1.2% basalt fiber. In addition, the fractal dimension of broken fragments presented in Figure 19 also reaches its minimum value under the basalt fiber content of 1.2%.

4. Conclusions

This research was performed to investigate the influence of basalt fiber on the static-dynamic mechanical characteristics and microstructure of cement-fly ash-stabilized soil. First, a

series of physical and mechanical experiments of cement-fly ash-stabilized soil were conducted to obtain the optimum mixed contents of cement and fly ash. After that, the static-dynamic mechanical behaviors and microstructure of basalt fiber-reinforced cement-fly ash-stabilized soil were studied by the unconfined compression test, SHPB test, and SEM test. Based on the results of this study, the following main conclusions can be drawn.

(1) Based on a series of physical and mechanical experiments of cement-fly ash-stabilized soil, the optimum mixed contents of cement and fly ash are considered as 5% cement and 10% fly ash.

(2) With the inclusion of basalt fiber, the static mechanical behaviors of cement-fly ash-stabilized soil are enhanced significantly. The unconfined compressive strength increases first and then decreases with an increase in the basalt fiber content. It can be found that the unconfined compressive strength of cement-fly ash-stabilized soil reaches it maximum value under the optimal basalt fiber dosage of 0.6%.

(3) The dynamic stress-strain curves of stabilized soil can be divided into three ordinal phases, namely, the approximate elastic deformation phase, plastic deformation phase, and failure phase. In contrast to the static stress-strain curve, the dynamic stress-strain curve has a similar ultimate strain under the same impact loading pressure.

(4) The improvement of dynamic mechanical properties of cement-fly ash-stabilized soil is a reason of the addition of basalt fiber. The dynamic compressive strength, dynamic increase factor (DIF), and specific energy absorption (SEA) of cement-fly ash-stabilized soil show an upward trend first and downward trend subsequently with basalt fiber content varying from 0% to 1.2%. With the basalt fiber content of 0.6%, the impact resistance and energy absorption capacity of cement-fly ash-stabilized soil can be enhanced effectively. What is more, the dynamic compressive strength, DIF, and SEA all show an increasing trend with the increase in impact loading pressure.

(5) The alteration of the failure patterns of stabilized soil under impact loading can be attributed to the addition of basalt fiber and the increasing impact loading pressure. The fractal dimension decreases gradually with an increase in basalt fiber content and increases correspondingly with the increase in impact loading pressure.

(6) The presence of cementitious products on the surfaces of basalt fibers and the formation of fiber-cemented soil matrix mixture can become the good interpretations to support the macroscopic mechanical behaviors. The generation of the stable internal space structure inside stabilized soil is the result of the addition of 0.6% basalt fiber into stabilized soil. Moreover, the fiber-fiber accumulated interfaces appear inside stabilized soil under the basalt fiber content of 1.2%.

Data Availability

The data used to support the findings of this study are available from the corresponding author upon request.

Conflicts of Interest

The authors declare that they have no conflicts of interest regarding the publication of this paper.

Acknowledgments

This research was supported by the Key Programs of Leading Talent Teams in Universities of Anhui Province (no. 2016_16). The authors wish to acknowledge the College of Civil Engineering and Architecture, Zhejiang University, for carrying out SEM tests.

References

[1] A. Seco, F. Ramírez, L. Miqueleiz, and B. García, "Stabilization of expansive soils for use in construction," *Applied Clay Science*, vol. 51, no. 3, pp. 348–352, 2011.

[2] A. K. Sharma and P. V. Sivapullaiah, "Ground granulated blast furnace slag amended fly ash as an expansive soil stabilizer," *Soils and Foundations*, vol. 56, no. 2, pp. 205–212, 2016.

[3] B. R. Phanikumar and R. S. Sharma, "Volume change behavior of fly ash-stabilized clays," *Journal of Materials in Civil Engineering*, vol. 19, no. 1, pp. 67–74, 2007.

[4] S. Saride, A. J. Puppala, and S. R. Chikyala, "Swell-shrink and strength behaviors of lime and cement stabilized expansive organic clays," *Applied Clay Science*, vol. 85, pp. 39–45, 2013.

[5] A. Kumar, B. S. Walia, and A. Bajaj, "Influence of fly ash, lime, and polyester fibers on compaction and strength properties of expansive soil," *Journal of Materials in Civil Engineering*, vol. 19, no. 3, pp. 242–248, 2007.

[6] Z. Nalbantoğlu, "Effectiveness of Class C fly ash as an expansive soil stabilizer," *Construction and Building Materials*, vol. 18, no. 6, pp. 377–381, 2004.

[7] A. K. Jha and P. V. Sivapullaiah, "Mechanism of improvement in the strength and volume change behavior of lime stabilized soil," *Engineering Geology*, vol. 198, pp. 53–64, 2015.

[8] M. Bekhiti, H. Trouzine, and M. Rabehi, "Influence of waste tire rubber fibers on swelling behavior, unconfined compressive strength and ductility of cement stabilized bentonite clay soil," *Construction and Building Materials*, vol. 208, pp. 304–313, 2019.

[9] F. S. Zha, S. Y. Liu, and Y. J. Du, "Experiment on improvement of expansive clays with lime-fly ash," *Journal of Southeast University (Natural Science Edition)*, vol. 37, no. 2, pp. 339–344, 2007.

[10] Y. Guney, D. Sari, M. Cetin, and M. Tuncan, "Impact of cyclic wetting-drying on swelling behavior of lime-stabilized soil," *Building and Environment*, vol. 42, no. 2, pp. 681–688, 2007.

[11] M. Al-Mukhtar, A. Lasledj, and J.-F. Alcover, "Behaviour and mineralogy changes in lime-treated expansive soil at 20°C," *Applied Clay Science*, vol. 50, no. 2, pp. 191–198, 2010.

[12] M. Al-Mukhtar, S. Khattab, and J.-F. Alcover, "Microstructure and geotechnical properties of lime-treated expansive clayey soil," *Engineering Geology*, vol. 139-140, pp. 17–27, 2012.

[13] A. R. Goodarzi, H. R. Akbari, and M. Salimi, "Enhanced stabilization of highly expansive clays by mixing cement and

silica fume," *Applied Clay Science*, vol. 132-133, pp. 675–684, 2016.

[14] E. Çokça, "Use of class C fly ashes for the stabilizationof an expansive soil," *Journal of Geotechnical and Geoenvironmental Engineering*, vol. 127, no. 7, pp. 568–573, 2001.

[15] B. R. Phani Kumar and R. S. Sharma, "Effect of fly ash on engineering properties of expansive soils," *Journal of Geotechnical and Geoenvironmental Engineering*, vol. 130, no. 7, pp. 764–767, 2004.

[16] K. Punthutaecha, A. J. Puppala, S. K. Vanapalli, and H. Inyang, "Volume change behaviors of expansive soils stabilized with recycled ashes and fibers," *Journal of Materials in Civil Engineering*, vol. 18, no. 2, pp. 295–306, 2006.

[17] R. S. Sharma, B. R. Phanikumar, and B. V. Rao, "Engineering behavior of a remolded expansive clay blended with lime, calcium chloride, and rice-husk ash," *Journal of Materials in Civil Engineering*, vol. 20, no. 8, pp. 509–515, 2008.

[18] B. R. Phanikumar and R. Singla, "Swell-consolidation characteristics of fibre-reinforced expansive soils," *Soils and Foundations*, vol. 56, no. 1, pp. 138–143, 2016.

[19] F. Yazdandoust and S. S. Yasrobi, "Effect of cyclic wetting and drying on swelling behavior of polymer-stabilized expansive clays," *Applied Clay Science*, vol. 50, no. 4, pp. 461–468, 2010.

[20] E. Kalkan, "Impact of wetting-drying cycles on swelling behavior of clayey soils modified by silica fume," *Applied Clay Science*, vol. 52, no. 4, pp. 345–352, 2011.

[21] M. Dayioglu, B. Cetin, and S. Nam, "Stabilization of expansive Belle Fourche shale clay with different chemical additives," *Applied Clay Science*, vol. 146, pp. 56–69, 2017.

[22] S. Por, S. Nishimura, and S. Likitlersuang, "Deformation characteristics and stress responses of cement-treated expansive clay under confined one-dimensional swelling," *Applied Clay Science*, vol. 146, pp. 316–324, 2017.

[23] C. J. Zhao, H. H. Zhao, Y. Chang, and B. W. Gong, "Physical-chemical experimental investigation on cement-treated highly expansive soil," *Journal of Dalian University of Technology*, vol. 54, no. 6, pp. 604–611, 2014.

[24] M. Liu, J. P. Song, J. Liu, and Y. F. Zhou, "Uniformity of cement-improved expansive soil in mixing technology," *Chinese Journal of Geotechnical Engineering*, vol. 39, no. S1, pp. 59–63, 2017.

[25] X. Li, Q. G. Cheng, J. C. Zhang, and Y. Yao, "Experimental study on dynamic performance of cement-improved expansive soil in high speed railway subgrade in wetting-drying cycles," *Railway Engineering*, vol. 2016, no. 6, pp. 99–103, 2016.

[26] S. R. Kaniraj and V. G. Havanagi, "Compressive strength of cement stabilized fly ash-soil mixtures," *Cement and Concrete Research*, vol. 29, no. 5, pp. 673–677, 1999.

[27] Q. Y. Ma and C. H. Gao, "Effect of basalt fiber on the dynamic mechanical properties of cement-soil in SHPB test," *Journal of Materials in Civil Engineering*, vol. 30, no. 8, Article ID 04018185, 2018.

[28] Z. W. Zhu, J. G. Ning, and X. Liu, "Dynamic mechanical behaviors of soil under impact loads," *Chinese Journal of High Pressure Physics*, vol. 25, no. 5, pp. 444–450, 2011.

[29] M. L. Yang, S. X. Chen, Y. Y. Quan, and C. H. Yuan, "Experimental research on improved expansive soil with lime in test section of the new Hankou airfield," *Chinese Journal of Rock Mechanics and Engineering*, vol. 25, no. 9, pp. 1868–1875, 2006.

[30] China Planning Press, *Ministry of Construction of the People's Republic of China, GB/T 50123-1999 Standard for Soil Test Method*, China Planning Press, Beijing, China, 1999, in Chinese.

[31] American Society for Testing and Materials (ASTM), *ASTM C 618-03, Standard Specification for Coal Fly Ash and Raw or Calcined Natural Pozzolan for Use as a Mineral Admixture in Concrete*, Annual Book of ASTM Standards, Philadelphia, PA, USA, 2003.

[32] X. Qin, A. Shen, Y. Guo, Z. Li, and Z. Lv, "Characterization of asphalt mastics reinforced with basalt fibers," *Construction and Building Materials*, vol. 159, pp. 508–516, 2018.

[33] Q. Y. Ma and Z. M. Cao, "Experimental study on fractal characteristics and energy dissipation of stabilized soil based on SHPB test," *Journal of Materials in Civil Engineering*, vol. 31, no. 11, Article ID 04019264, 2019.

[34] P. Yuan and Y. Xu, "Influence of curing time on impact energy absorption characteristics of artificially cemented sand," *Journal of Vibroengineering*, vol. 19, no. 6, pp. 4033–4041, 2017.

[35] Y. R. Lyu, M. Y. Wang, J. Q. Wei, and B. Liao, "Experimental techniques of SHPB for calcareous sand and its dynamic behaviors," *Explosion and Shock Waves*, vol. 38, no. 6, pp. 1262–1270, 2018.

[36] Y. G. Miao, Y. L. Li, Q. Deng, Z. B. Tang, H. T. Hu, and T. Suo, "Investigation on experimental method of low-impedance materials using modified Hopkinson pressure bar," *Journal of Beijing Institute of Technology*, vol. 24, no. 2, pp. 269–276, 2015.

[37] C. H. Gao, Q. Y. Ma, and D. D. Ma, "SHPB test and analysis on cemented silty clay under confining pressure conditions," *Journal of Vibration and Shock*, vol. 37, no. 14, pp. 162–167, 2018.

[38] Q. Y. Ma, Z. M. Cao, and P. Yuan, "Experimental research on microstructure and physical-mechanical properties of expansive soil stabilized with fly ash, sand, and basalt fiber," *Advances in Materials Science and Engineering*, vol. 2018, Article ID 9125127, 13 pages, 2018.

[39] P. Jamsawang, T. Suansomjeen, P. Sukontasukkul, P. Jongpradist, and D. T. Bergado, "Comparative flexural performance of compacted cement-fiber-sand," *Geotextiles and Geomembranes*, vol. 46, no. 4, pp. 414–425, 2018.

[40] X. S. Zhuang and X. Y. Yu, "Experimental study on strength of expansive soil treated by lime-basalt fiber," *China Civil Engineering Journal*, vol. 48, no. S1, pp. 166–170, 2015.

[41] H. Su and J. Xu, "Dynamic compressive behavior of ceramic fiber reinforced concrete under impact load," *Construction and Building Materials*, vol. 45, pp. 306–313, 2013.

[42] L. Gao, G. H. Hu, N. Xu, J. Y. Fu, C. Xiang, and C. Yang, "Experimental study on unconfined compressive strength of basalt fiber reinforced clay soil," *Advances in Materials Science and Engineering*, vol. 2015, Article ID 561293, 8 pages, 2015.

[43] A. Macías-García, E. M. Cuerda-Correa, and M. A. Díaz-Díez, "Application of the Rosin-Rammler and Gates-Gaudin-Schuhmann models to the particle size distribution analysis of agglomerated cork," *Materials Characterization*, vol. 52, no. 2, pp. 159–164, 2004.

[44] J. S. Shi, J. Y. Xu, W. B. Ren, and H. Y. Su, "Research on energy dissipation and fractal characteristics of concrete after exposure to elevated temperatures under impact loading," *Acta Armamentarii*, vol. 35, no. 5, pp. 703–710, 2014.